Carbon Dioxide Separation with

Novel Microporous Metal Organic Frameworks

Final Technical Report

Reporting Start Date: 5 August 2004

Reporting End date: 4 February 2008

Richard Willis, *Annabelle Benin, John Low, Ganesh Venimadhavan, Syed Faheem, David Lesch*
UOP LLC, a Honeywell Company
25 E. Algonquin Road
Des Plaines, IL 60017-5016
Phone: (847) 391-3190; Fax: (847) 391-3719; E-mail: Richard.Willis@uop.com

Report Issued: April 2008

Contract Number: DE-FG26-04NT42121

Subcontractors:
Adam Matzger, University of Michigan, Ann Arbor, MI
Randy Snurr, Northwestern University, Evanston, IL

DISCLAIMER

This report was prepared as an account of work sponsored by an agency of the United States Government. Neither the United States Government nor any agency thereof, nor any of their employees, makes any warranty, express or implied, or assumes any legal liability or responsibility for the accuracy, completeness, or usefulness of any information, apparatus, product, or process disclosed, or represents that its use would not infringe privately owned rights. Reference herein to any specific commercial product, process, or service by trade name, trademark, manufacturer, or otherwise does not necessarily constitute or imply its endorsement, recommendation, or favoring by the United States Government or any agency thereof. The views and opinions of authors expressed herein do not necessarily state or reflect those of the United States Government or any agency thereof.

ABSTRACT

The goal of this program was to develop a low cost novel sorbent to remove carbon dioxide from flue gas and gasification streams in electric utilities. Porous materials named metal-organic frameworks (MOFs) were found to have good capacity and selectivity for the capture of carbon dioxide. Several materials from the initial set of reference MOFs showed extremely high CO_2 adsorption capacities and very desirable linear isotherm shapes. Sample preparation occurred at a high level, with a new family of materials suitable for intellectual property protection prepared and characterized. Raman spectroscopy was shown to be useful for the facile characterization of MOF materials during adsorption and especially, desorption. Further, the development of a Raman spectroscopic-based method of determining binary adsorption isotherms was initiated. It was discovered that a stronger base functionality will need to be added to MOF linkers in order to enhance CO_2 selectivity over other gases via a chemisorption mechanism. A concentrated effort was expended on being able to accurately predict CO_2 selectivities and on the calculation of predicted MOF surface area values from first principles. A method of modeling hydrolysis on MOF materials that correlates with experimental data was developed and refined. Complimentary experimental data were recorded via utilization of a combinatorial chemistry heat treatment unit and high-throughput X-ray diffractometer. The three main Deliverables for the project, namely (a) a MOF for pre-combustion (e.g., IGCC) CO_2 capture, (b) a MOF for post-combustion (flue gas) CO_2 capture, and (c) an assessment of commercial potential for a MOF in the IGCC application, were completed. The key properties for MOFs to work in this application - *high CO_2 capacity*, *good adsorption/desorption rates*, *high adsorption selectivity* for CO_2 over other gases such as methane and nitrogen, *high stability to contaminants*, namely moisture, and *easy regenerability*, were all addressed during this program. As predicted at the start of the program, MOFs have high potential for CO_2 capture in the IGCC and flue gas applications.

Table of Contents

1. INTRODUCTION…… 4

2. EXECUTIVE SUMMARY…….. 5

3. EXPERIMENTAL……... 6

4. RESULTS AND DISCUSSION…….. 8

4.1 Isotherm Generation……..... 8

4.2 MOF Synthesis…… 12

4.2.1 Reference MOFs and other Zn-containing MOFs……. 12

4.2.2 Cu-BTC……. 14

4.2.3 Amino-functionalized MOFs……... 15

4.2.4 Smaller Pore Size MOFs…….. 17

4.2.5 Synthesis of MOFs with Mixed Linkers…… 18

4.2.6 Scale up and forming of MOFs……. 24

4.3 Molecular Modeling/ Virtual High-Throughput Screening…… 25

4.3.1 General Molecular Modeling Considerations……. 25

4.3.2 MOF Surface Areas…… 29

4.3.3 Virtual High Throughput Screening…….. 30

4.3.4 Modeling Hydrolysis……. 32

4.4 Hydrothermal and Other Contaminant Stability……. 37

4.5 Commercial Issues…….. 40

4.5.1 Background…… 40

4.5.2 Techno-economic Evaluation of MOFs for IGCC CO_2 Capture… 41

5. CONCLUSIONS…….. 46

6. REFERENCES……. 48

1 INTRODUCTION

UOP LLC, Northwestern University (NU) and the University of Michigan (UM) collaborated on a three-year program to discover novel microporous metal organic frameworks (MOFs) suitable for CO_2 capture applications. This innovative program combined sophisticated molecular modeling with the structural diversity of the highly porous, thermally stable MOFs, which have been shown to possess exceptional storage capacity for methane, hydrogen, and other gases. Selected MOFs were optimized for CO_2 selectivity, adsorption capacity, and adsorption and desorption rates. The successful completion of this program has pointed us toward MOFs as low cost, novel adsorbents to remove CO_2 from flue gas and gasification streams in electric utilities, likely via a pressure swing adsorption (PSA) process. Utilization of MOFs in these applications will allow the use of fossil fuels as energy sources without contributing to global warming.

The project end date was 4 February 2008. Professor Adam Matzger served as the principal investigator at UM, where MOFs were prepared and adsorption properties measured. UOP's role, which was expanded significantly from the role originally proposed, included conducting MOF hydrothermal stability tests, performing MOF syntheses based on open literature preparations, and in developing predictive models on MOF sensitivity to moisture in the gas streams. Meanwhile, the modeling of gas adsorption isotherms and predictions of novel MOF surface area values, carried out under the direction of Professor Randy Snurr at NU, helped accelerate more rapid synthesis and characterization at UM and UOP.

The MOFs are structurally and chemically diverse, and well over 700 materials have been prepared. [1 2 3] In late 2006, the proposed technical approach was modified to allow the use of molecular modeling to identify MOFs with the best sorption properties for CO_2. In early to mid-2007, the team was to select the best MOF to scale-up for more detailed commercially relevant testing. IRMOF-1 and MIL-53 were identified as MOFs that could work in the integrated gas combined-cycle (IGCC) application, and these materials and others were scaled up to the 'tens of grams' level. Process economics and process integration for the CO_2 capture part of the IGCC application were addressed near the end of the project.

2 EXECUTIVE SUMMARY

UOP LLC, Northwestern University (NU) and the University of Michigan (UM) collaborated on a three-year program to discover novel microporous metal organic frameworks (MOFs) suitable for CO_2 capture applications. This innovative program combined sophisticated molecular modeling with the structural diversity of the highly porous, thermally stable MOFs, which have been shown to possess exceptional storage capacity for methane, hydrogen, and other gases. Selected MOFs were optimized for CO_2 selectivity, adsorption capacity, and adsorption and desorption rates. The successful completion of this program has pointed us toward a low cost, novel adsorbent to remove CO_2 from flue gas and gasification streams in electric utilities, likely via a pressure swing adsorption (PSA) process. Utilization of MOFs in these applications will allow the use of fossil fuels as energy sources without contributing to global warming.

During Phase 1 of the program, a broad scoping study was performed where existing MOFs were evaluated for CO_2, CH_4, and N_2 sorption such that a theoretical Virtual High Throughput Screening (VHTS) model could be developed and verified. A good VHTS model should allow for the design of novel MOFs with improved sorption properties for CO_2. A variety of MOFs were selected to parameterize the model. The initial set of reference MOFs consisted of IRMOF-1, the parent structure of the isoreticular metal organic framework (IRMOF) series, IRMOF-3, an amino-functionalized derivative of IRMOF-1, and MOFs possessing different building units: MOF-2 (square channels), MOF-74 (hexagonally packed cylindrical channels), and MOF-177 (ultra-high porosity framework). IRMOF-6 is sometimes included with the set of reference MOFs owing to its similarity in surface area and other properties to the amino-substituted IRMOF-3. It was found that the shape of a given isotherm curve and maximum gas uptake can be tuned by varying the MOF structure. Of the materials tested, MOF-177, which has the highest surface area, had the highest capacity for CO_2 at 195K at low pressure and at 298K and high pressure. Meanwhile, a VHTS model was developed to predict isotherms for CO_2 on MOFs. The model successfully predicted isotherms for N_2 on IRMOF-1 and IRMOF-3 as well.

During the first half of Phase 2, several extensions of the work from Phase 1 were carried out. Methane single component isotherm generation on the selected MOFs was completed, and results showed a lower capacity for methane versus CO_2. In other words, the MOFs had a higher selectivity for CO_2 over methane. In order to gain insight into selectivity issues, a new adsorption cell was constructed and methane/ CO_2 binary adsorption measurements were conducted. Results for IRMOF-1, which were verified by Raman spectroscopy, showed a significant adsorptive selectivity for CO_2 over methane. The reversibility of pure high pressure CO_2 adsorption isotherms measurements was also verified, and adsorption/desorption rates were found to be acceptably short. Additionally, two new amine-substituted MOFs were synthesized, characterized and modeled for CO_2 adsorption. Molecular modeling studies and calculations provided isotherms that correlated very closely to those obtained experimentally. Calculations also provided insight into the unusual inflection points in several of the isotherms.

During the latter half of the program, significant progress toward a fundamental understanding of the characteristics required for a MOF suitable for IGCC and flue gas operation were achieved. In addition, we have suggested several MOFs suitable for the

IGCC application. Among our findings was a method for molecular modeling of a hydrolysis reaction on MOF materials that correlates with experimental data. The experimental data were generated via a combinatorial chemistry heat treatment unit and high-throughput X-ray diffractometer. Sample preparation occurred at a high level at UOP and UM, with the latter developing a new family of materials suitable for intellectual property protection. UM researchers also continued the development of a Raman spectroscopic-based method of determining binary adsorption isotherms. NU researchers concentrated on being able to accurately predict CO_2 selectivities and the calculation of predicted MOF surface area values from first principles. An assessment of the commercial potential use of MOFs for CO_2 capture in the IGCC application was carried out near the end of the project.

Some preliminary conclusions can be drawn from the MOF/ PSA (pressure swing adsorption) in IGCC commercial feasibility study. First, the cost impact of the MOF/PSA process on the overall CO_2 capture and compression will not be significant because it is only one of many processes that are necessary for capturing CO_2. However, MOFs will eliminate the use of potentially hazardous solvents in CO_2 capture. There is also significant promise on the power used/lost front. Additional improvement could include reuse of CO_2 at lower pressures, better energy integration and optimization of the entire IGCC with CO_2 capture process to best match energy sources and sinks, co-sequestration of CO_2, H_2S and COS, and lower purity requirements for CO_2 reuse processes.

The three main Deliverables for the project were (a) a MOF for pre-combustion (e.g., IGCC) CO_2 capture, (b) a MOF for post-combustion (flue gas) CO_2 capture, and (c) an assessment of the commercial potential for a MOF in the IGCC application. IRMOF-1, in a bone dry stream, or MIL-53 in a moisture-saturated stream, are two MOFs which could work satisfactorily for the IGCC application. MIL-53 or MOF-74 could work in the flue gas application, but additional work needs to be done to continue the search for an even better low temperature/ low pressure adsorbent.

3 EXPERIMENTAL

The activated porous materials were handled under a blanket of nitrogen or methane gas. Detailed MOF synthesis procedures were provided in the Phase 1 report. An example for one of the original six materials, MOF-177, is provided here: $Zn(NO_3)_2{\cdot}6H_2O$ (0.368 g) and 4,4',4"-benzene-1,3,5-triyl-tri-benzoic acid (H_3BTB) (0.180 g) were dissolved in DEF (10 mL) in a 20 mL vial, capped tightly, and heated to 100 °C for 20 hours. The solution was decanted, and the clear block crystals were washed in DMF and exchanged with $CHCl_3$ thrice in three days. The material was evacuated at 125 °C for 6 hours to give a 4508 m^2/g sample. The MOF-177 crystallographic backbone density of 1.22 g/cm^3 was used to obtain its volumetric capacity. The backbone density was determined from the quotient of the guest-free unit cell formula weight (9180.45 g/mol) and the framework (backbone) volume. The framework volume was calculated as the difference between the unit cell volume and the “accessible” pore volume from Cerius2. Surface areas were

determined with a single-point BET model from N_2 adsorption data collected at 77 K on either a gravimetric system, or an Autosorb-1C. New MOFs, IRMOF-31 and IRMOF-32, were prepared in similar fashion to MOF-177, except that IRMOF-31 reacted with the secondary amine substituted bis dicarboxylate linker at 85 ^{o}C in DEF for 3 days, and IRMOF-32 was formed by reaction of the tertiary amine substituted linker at 85 ^{o}C for 4 days. Experimental details for UMCM-1 can be found elsewhere[4]. All other procedures were the same or similar.

The gravimetric uptake capacity of carbon dioxide for each MOF was determined by exposing an evacuated sample of the MOF adsorbent to increasing pressure increments of carbon dioxide gas at ambient temperature. The sample and gas were allowed to come to equilibrium for each of the increments, at which point the corresponding weight change was recorded, corrected for buoyancy, and plotted versus pressure. Similar procedures were used for obtaining nitrogen and methane isotherm data.

In order to perform binary gas adsorption isotherm measurements, a sample cell had to be constructed. Once the cell was built, several pressure tests were performed to search for leaks in the cell. For each pressure test the cell was charged with 400-500 PSI of N_2 into both chambers and the pressure was monitored over time. Leak testing was performed until a satisfactory leak rate was observed (< 0.05 psi/min). After successful leak testing, adsorption analysis was started.

For hydrothermal stability testing, the solvent-exchanged, dried MOF material is used as received (if in powder form) or placed through a mesh screen if the material contains chunks. A small quantity (< ½ cm height) is loaded into each of the quartz tubes and the material is heated to a specified temperature overnight in flowing nitrogen. The tubes are allowed to cool to the designated steam temperatures, and steam (in nitrogen) is introduced at the desired level for 2 hours. Each tube is maintained at 60 °C in the absence of steam for 1 hour before being quickly removed from the oven and loaded into a GADDs plate. X-ray powder diffraction data were collected either on a Bruker AXS GADDS diffractometer, which is equipped with an automated XYZ stage for sample positioning. Data were collected over the 2Θ range from at least 4°-35°, in 0.05° steps via 30 second scans.

4 RESULTS AND DISCUSSION

The first year of the program was characterized by a broad scope study where existing MOFs were evaluated for CO_2, CH_4, and N_2 sorption such that a theoretical Virtual High Throughput Screening (VHTS) model could be developed and verified. The VHTS model was to allow for the design of novel MOFs with improved sorption properties. Therefore, a goal in the first year was to identify MOFs to parameterize the VHTS model. Six reference MOFs that represent broad structural and functional diversity, IRMOF-1, IRMOF-3, IRMOF-6, MOF-2, MOF-74, and MOF-177, were selected for initial evaluation. IRMOF-1 is the parent structure of the isoreticular metal organic framework (IRMOF) series and has been the most extensively studied MOF. The selected MOFs are shown in **Figure 1.**

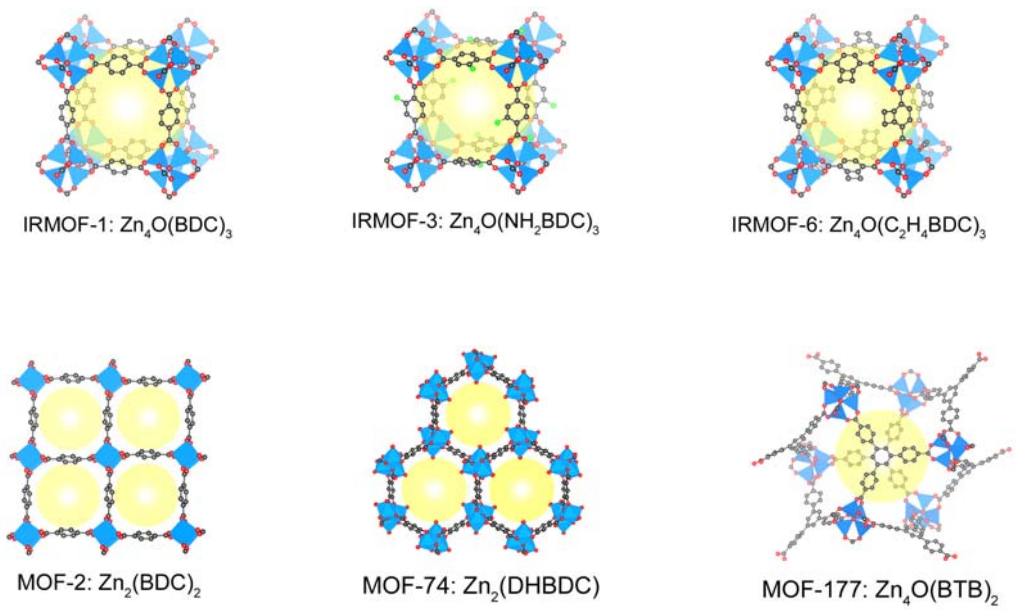

Figure 1. Reference MOFs selected for detailed evaluation in Phase 1 of the program.

4.1 Isotherm Generation

Room-temperature high pressure carbon dioxide adsorption isotherms are shown in **Figure 2** and some key parameters are summarized in **Table 1**. MOF-2 has a typical monotonic isotherm (Type I) where the more intense gas adsorption at low pressure forms a "knee" in the isotherm. This same shape for the low-temperature (195 K) MOF-2 isotherm was found when carbon dioxide sorption was first reported in MOFs. Similarly, for the room temperature isotherm the pores begin to saturate at higher pressure and the uptake reaches a plateau. This results in a capacity of 3.2 mmol carbon dioxide per g MOF-2. Likewise, MOF-74 has a similar isotherm shape, but the capacity of this material is much greater owing to a larger micropore volume. The saturation capacity is 10.4 mmol/g. On the other hand, IRMOF-3, and IRMOF-1 show substantially greater

capacities for carbon dioxide than the other two MOFs, having corresponding uptakes of 18.7 and 21.8 mmol/g. Significantly, the shapes of these isotherms gradually take on a sigmoidal curve (referred to as a step) with increasing capacity. The appearance of the step in this pressure regime is due to larger pore sizes, which allow the behaviour of the gas to resemble the phase diagram of the bulk fluid. The voluminous space enclosed by MOF-177 enables it to adsorb carbon dioxide up to 33.7 mmol/g.

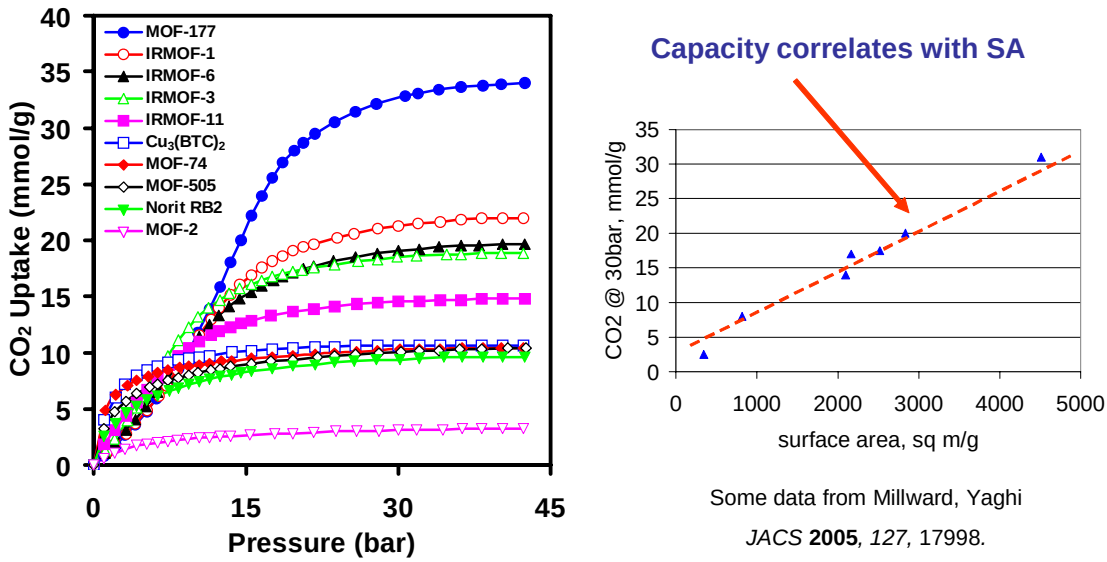

Figure 2. CO_2 adsorption isotherms for reference MOFs and plot showing correlation of CO_2 capacity and MOF surface area.

Table 1. Some reference MOF adsorption details.

	Formula Unit	Uptake (mmol/g) at 35 bar	# CO_2 per Formula Unit	Surface Area (m^2/g)	Step Maximum (bar)
MOF-2	$Zn_2(BDC)_2$	3.2	1.5	345	<5
MOF-74	$Zn_2(DHBDC)$	10.4	3.4	816	<5
IRMOF-3	$Zn_4O(NH_2BDC)_3$	18.7	15.2	2160	6.2
MOF-5	$Zn_4O(BDC)_3$	21.7	16.7	2833	10.4
MOF-177	$Zn_4O(BTB)_2$	33.5	38.5	4508	14.5

A major scientific and technical challenge in this project was the need for a way to determine the adsorption behavior of MOFs in presence of a mixture of gases. The typical assumption made in predicting binary adsorption behavior, namely that each gas will adsorb independently, seemed suspect because at high loadings there is more mass of

sorbed gas than of actual sorbent suggesting that adsorption behavior would be significantly perturbed. Our earlier approach to this problem involved using mass spectrometry to look at gas evolution from MOF samples at high pressure. This gave reasonable qualitative results, reflecting selectivity differences, but was unable to produce an isotherm that would be useful for predicting behavior quantitatively at an arbitrary pressure. This technique also has quite demanding sample requirements. We have now solved this problem with a conceptually unique approach employing Raman spectroscopy that can yield single or multiple components isotherms on milligram quantities of samples.

To illustrate the approach, results are given in **Figure 3** for the single component isotherm for CH_4 desorption in IRMOF-1 at room temperature. This is derived by fitting the peak corresponding to the vibrational mode of the gas adsorbed in the MOF and comparing this intensity to a MOF framework peak. Because the MOF framework peak should not change as a function of pressure, this allows ratiometric determination of the absolute amount of gas adsorbed at any pressure using a single point calibration against a known uptake. The use of desorption is operationally convenient and yields that same results as adsorption due to the lack of hysteresis in the room temperature adsorption isotherms. Benchmarking the isotherm against gravimetric sorption data is crucial to demonstrate that an isotherm derived from Raman spectroscopy is reliable and therefore the data are overlaid in **Figure 3** showing good agreement. Corresponding data for CO_2 in IRMOF-1 are provided as **Figure 4**. Some deviation is observed at very high pressures and this may well be due to the fact that Raman spectroscopy measures the total quantity of the adsorbed phase rather than the Gibbs excess derived in a more traditional gravimetric or volumetric experiment. This is a minor point that can be corrected for in the future if necessary.

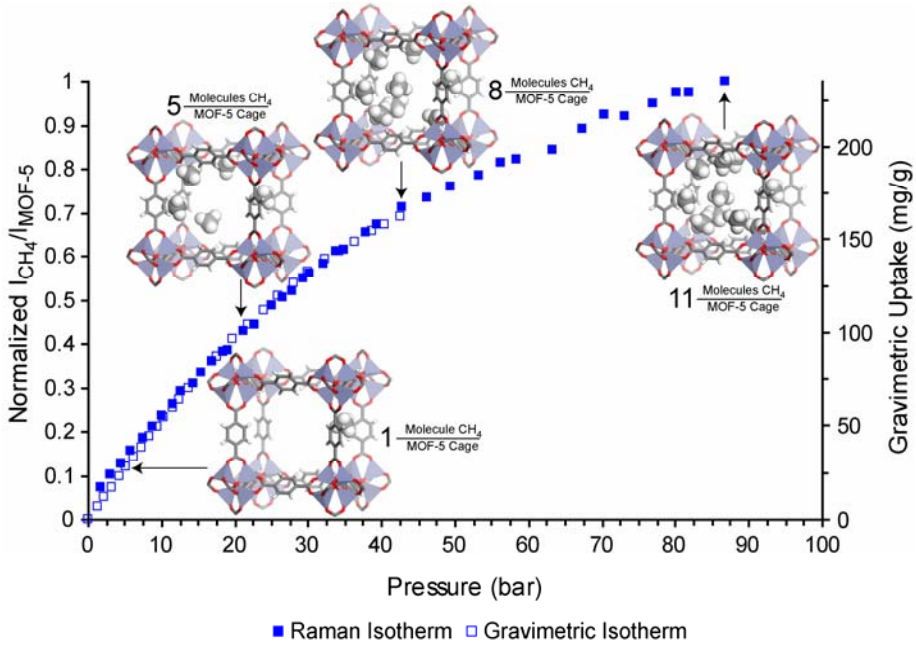

Figure 3. Methane adsorption isotherms generated via Raman adsorption spectroscopy and gravimetric methods on IRMOF-1 at room temperature.

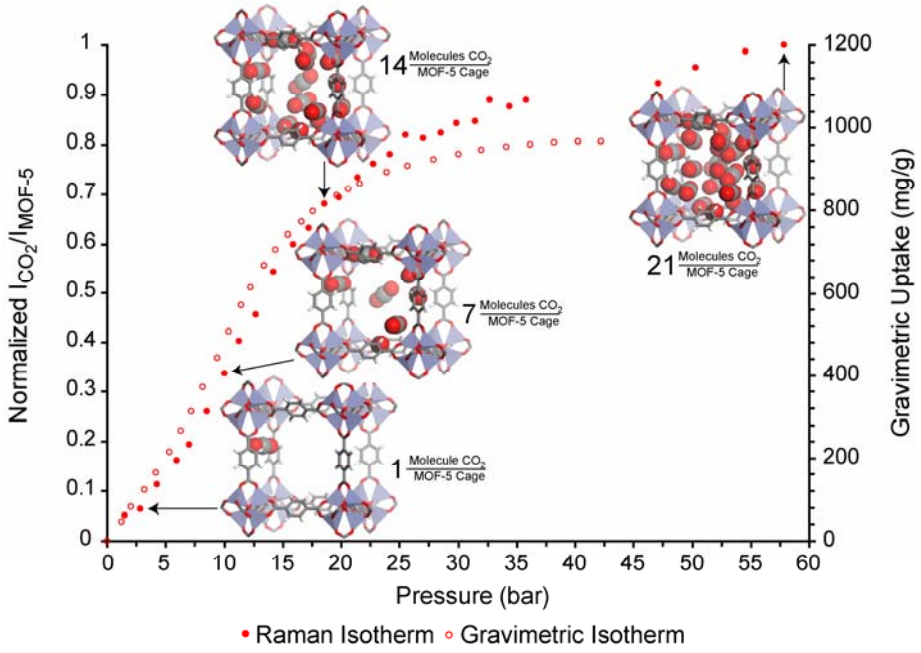

Figure 4. CO_2 adsorption isotherms generated via Raman adsorption spectroscopy and gravimetric methods on IRMOF-1 at room temperature.

For the binary gas adsorption experiment, a 1:1 mixture of CH_4/CO_2 was chosen. At low pressure this follows the general expectation from single component isotherm additively. Significantly, at high pressure, large deviations from the ideal picture are seen (**Figure 5**).

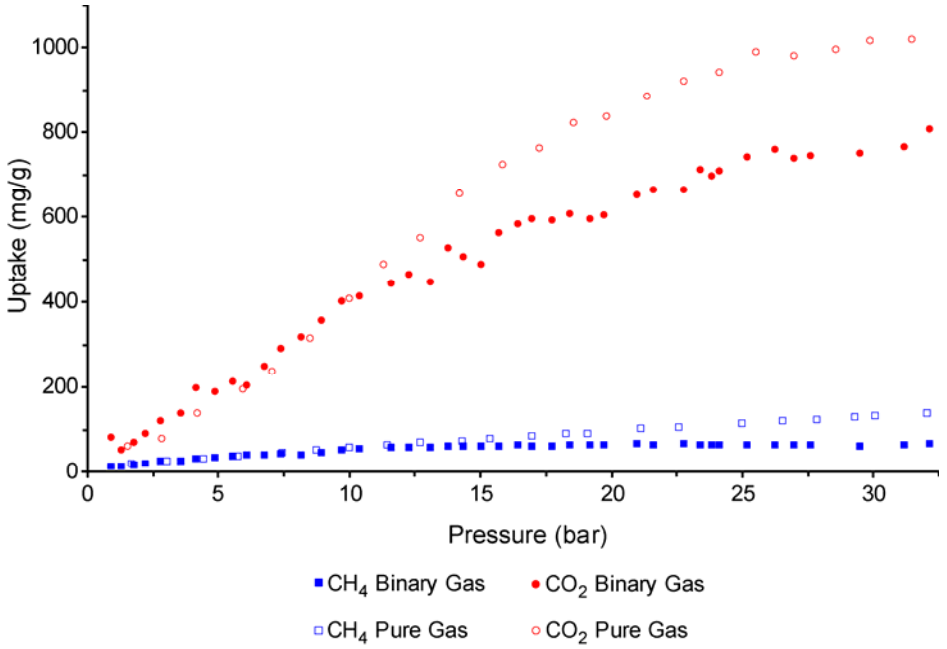

Figure 5. Comparison of IRMOF-1 uptake vs. partial pressure of gas for both single component and 1:1 mixtures of methane and CO_2.

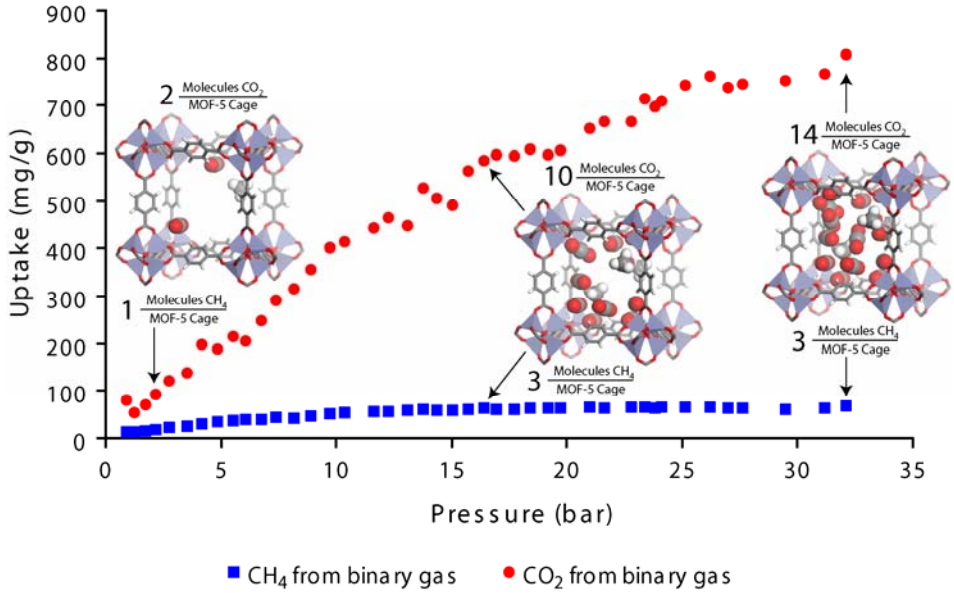

Figure 6. Isotherms for CH_4 and CO_2 sorption in IRMOF-1 plotting uptake vs. partial pressure. The inset chemical structures illustrate the loading associated with each mass uptake point indicated by the arrows.

For example, methane adsorption, instead of increasing continually to >90 bar, is essentially saturated at 15 bar partial pressure. CO_2 adsorption, however, continues to climb over the whole isotherm. A key result from these studies is that the ratio of adsorbed CH_4 to CO_2 could not be predicted without experimental determination of the binary gas adsorption behavior and that in different pressure regimes the selectivity for each gas can be determined. **Figure 6** illustrates this point.

The future outlook for this technique is quite promising. It displays its best sensitivity in the high pressure region, where deviation from an ideal model assuming additivity of the two single component isotherms breaks down most dramatically. It can be adapted to essentially all diatomic and higher gases in binary mixtures and should be equally applicable to ternary and higher mixtures with appropriate adjustment of spectral collection time.

4.2 MOF Synthesis

4.2.1 Reference MOFs and other Zn-containing MOFs

The early synthetic work involved investigating

the use of prototypical highly porous MOFs, and in particular, the IRMOF series based on IRMOF-1. The IRMOF-1 material is readily prepared from a mixture of a zinc salt and a bis-dicarboxylic acid, and derivatives of IRMOF-1 can be readily prepared by functionalizing the bis-dicarboxlyate linker. Amines have proven to be excellent functional groups for reversible CO_2 storage on other materials and could be expected to significantly enhance the sorption properties of MOFs for CO_2. The dicarboxlyate linker can be readily substituted with amines (**Figure 7**). The ability to vary the substituents on the aromatic ring may give rise to materials with varying capacities whereas the ability to introduce amines with varying nucleophilicities could give rise to sorbents with different binding energies.

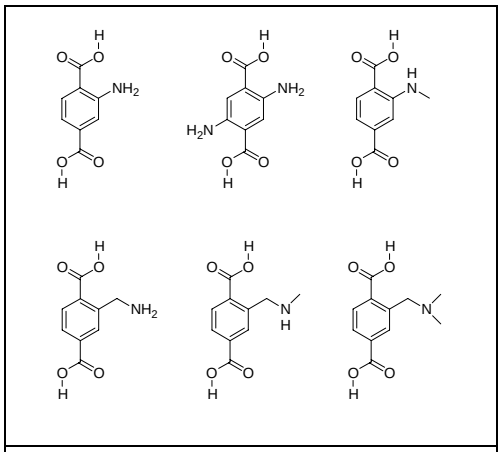

Figure 7. Some amino-functionalized bis-dicarboxylic acid linkers

Another of our objectives was to prepare MOFs based upon open literature synthetic methods in order to gain experience in the preparation of a broad spectrum of MOF materials. This is because it is likely that we will need to move away from 4-coordinate, coordinatively unsaturated zinc clusters as the inorganic 'cornerstone' building unit in order to enhance hydrothermal stability. For example, as will be discussed later in the report, 6-coordinate Zn-containing MOF-74 is significantly more hydrothermally stable than all four-coordinate Zn-containing IRMOF series compounds. Five-coordinate Zn-containing MOFs (e.g., MOF-508 and Zn-IDC) possess hydrothermal stability intermediate between the IRMOF series and MOF-74. Some Zn-containing MOFs in various coordination environments are shown in **Figure 8.**

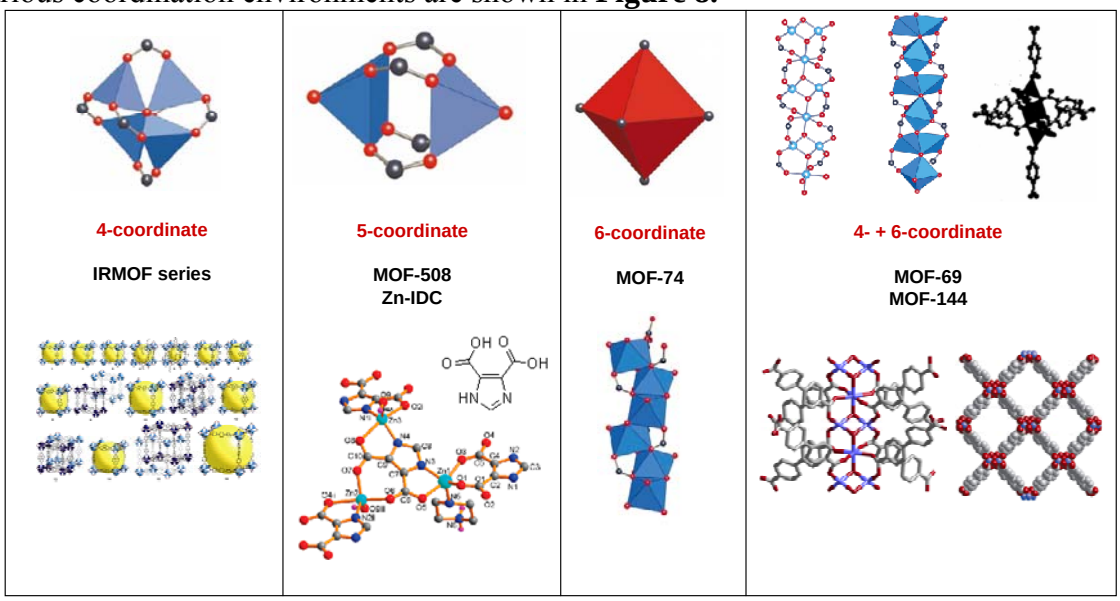

Figure 8. Different zinc-MOF coordination environments.

4.2.2 Cu-BTC

We identified several other metal-organic materials from the open literature that show reasonable measured CO_2 capacity and additionally would be expected to be more hydrothermally stable than our current set of reference zinc-containing MOFs. An example of one of these materials is H-KUST-1, also known as Cu-BTC[5].

Cu-BTC Synthesis details are provided as **Figure 9**. Thermal stability of Cu-BTC (~ 300 ^{o}C) was determined by TGA and X-ray diffraction (XRD) analyses (**Figure 10**).

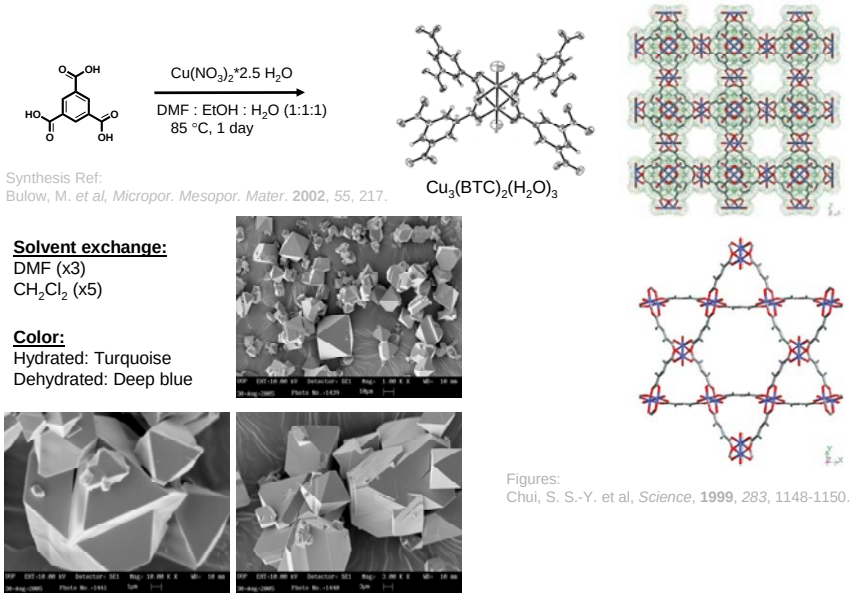

Figure 9. Synthesis and characterization of Cu-BTC.

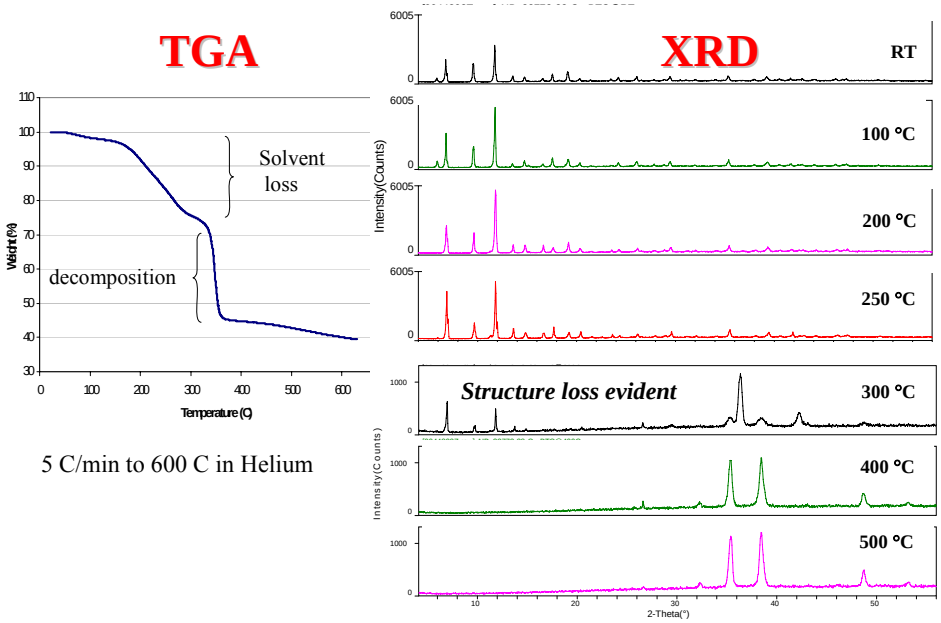

Figure 10. Thermal gravimetric (TGA) and X-ray diffraction (XRD) results for Cu-BTC.

The existence of coordinatively unsaturated metal sites was confirmed by low temperature carbon monoxide (LT CO-FTIR) measurements (see **Figure 11**).

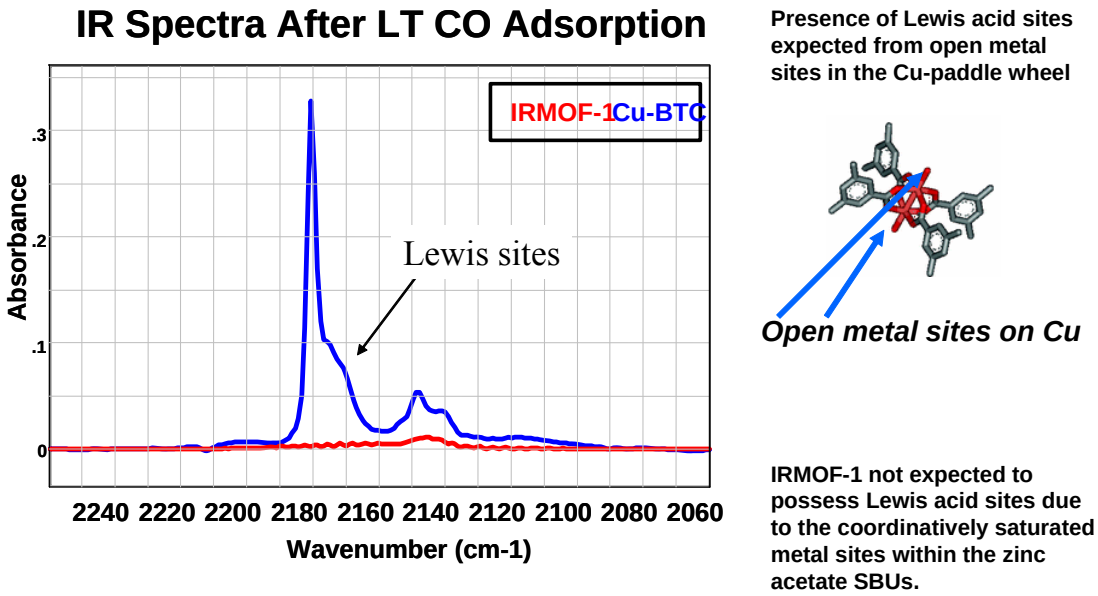

Figure 11. A) Low temperature CO adsorption FTIR spectrum for Cu-BTC and IRMOF-1. B) Lewis acid site description for Cu-BTC.

4.2.3 Amino-functionalized MOFs

One of the original goals of our work was to look at the effect of amine functionality on CO_2 uptake. In particular we proposed to explore the effect of degree of substitution, to probe electronic and steric contributions, by examining IRMOF-3 (Ar-NH_2) and IRMOF-31 (Ar-$NHCH_3$). Gas uptake in these compounds was measured up to 1 atmosphere at two temperatures (195 K and 273 K). Both IRMOF-3 and IRMOF-31 do not show chemisorption of CO_2 at 195 K and 273 K (judged by reversibility of adsorption **Figure 12**) or room temperature (Raman spectroscopy, not shown). Interestingly, however, the

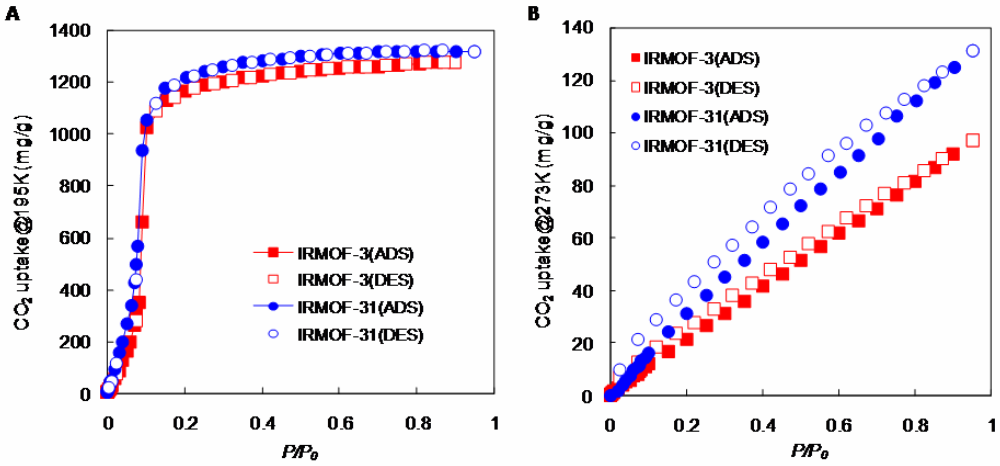

Figure 12. A. CO_2 uptake at 195K of IRMOF-3 and IRMOF-31. **B.** CO_2 uptake at 273K.

CO_2 uptake of IRMOF-31 shows much higher value than that of IRMOF-3 at 273 K, compared to the CO_2 uptake at 195 K (**Figure 12 B**). This result may follow from pore constriction by methyl groups of IRMOF-31. The decrease of pore dimension may have an impact on increasing the CO_2 uptake at comparatively low pressure region (under 1 atmosphere) and higher temperature (over 273 K). This provides us a pathway for increasing physisorption in MOFs.

We reported above the synthesis and CO_2 sorption behavior of IRMOF-3 (amine substituted IRMOF-1) and several derivatives that only possessed one amino group on each linker. Believing that this may not be sufficient amine density in the material to stabilize carbamic acid formation, we executed the synthesis of amine substituted MOFs derived from 4,4'-biphenyl dicarboxylic acid (**Scheme 1**).

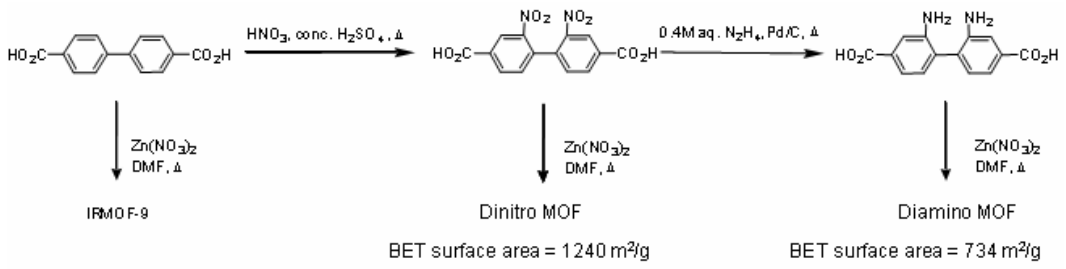

Scheme 1. Synthesis of dinitro- and diamino-substituted diphenyl dicarboxylate linkers and the corresponding MOFs.

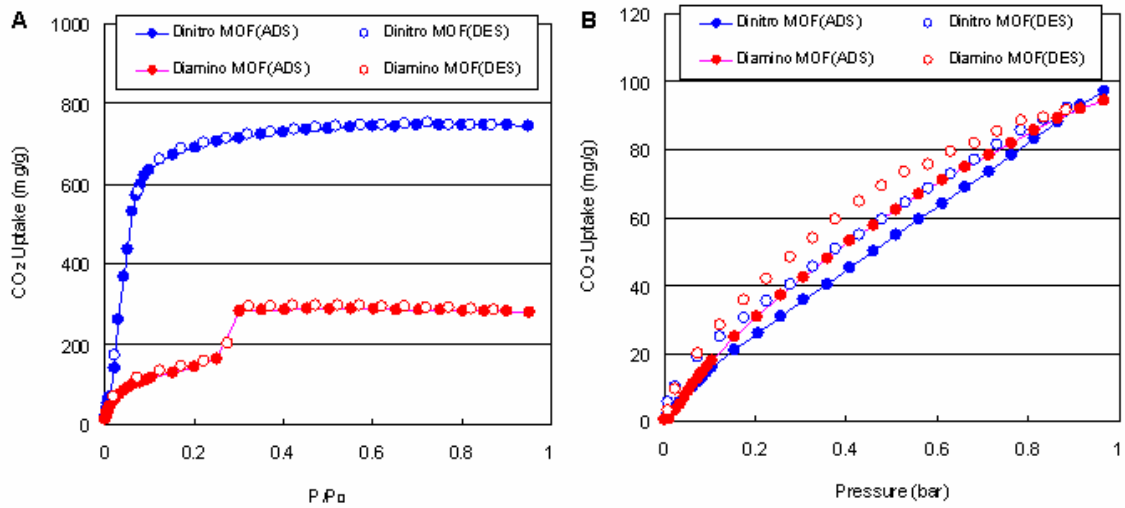

Figure 13. A) CO_2 uptake at 195K for Dinitro MOF and Diamino MOF. B) CO_2 uptake at 298K for the same two MOFs.

The MOFs derived from the dinitro- and diamino-substituted diphenyl dicarboxylic acid show moderate surface areas. Their moderate CO_2 uptake at both low temperature (195 K) and room temperature (**Figure 13**) suggests that only physisorption is taking place. The conclusion from these studies was that a stronger basic functionality in the linker will

be required to achieve chemisorption. Unfortunately, there are significant issues associated with synthesizing such materials at present.

4.2.4 Smaller Pore Size MOFs

Previous results have encouraged us to explore materials that, although possessing lower ultimate capacity for carbon dioxide, show higher CO_2 affinities at lower partial pressure and room temperature. In other words, stronger physisorpion in MOFs can be favored by using smaller pore materials and those with open metal sites such as MOF-74, a zinc-based material constructed from 2,5-dihydroxy-1,4-benzene dicarboxylic acid and zinc nitrate tetrahydrate. The structure of MOF-74 contains one-dimensional hexagonal channels in which infinite chains of zinc atoms are linked together by the tetra-anion of 2,5-dihydroxy-1,4-benzene dicarboxylic acid. The diameter of the channel is approximately 12 Å, taking into account the Van der Waals radii of the atoms. **Figure 14** shows the CO_2 sorption isotherm for MOF-74, where at approximately 1 atm, the material takes up nearly about 20 wt% of CO_2 gas at room temperature (or nearly 5 wt% capacity at 0.1 atm pressure). Co-MOF-74 and Ni-MOF-74, are isostructural materials that likewise contain open metal sites. These are of interest because each has a higher surface area than Zn-MOF-74, and both may be more stable to water and/or steam exposure. Two different synthetic methods were used to obtain Co-MOF-74, and Ni-MOF-74 was successfully prepared as well. These materials were not fully evaluated by the end of the project period, but will be examined in detail in the second DOE/NETL sponsored programmed administered by UOP LLC (DE-FC26-07NT43092).

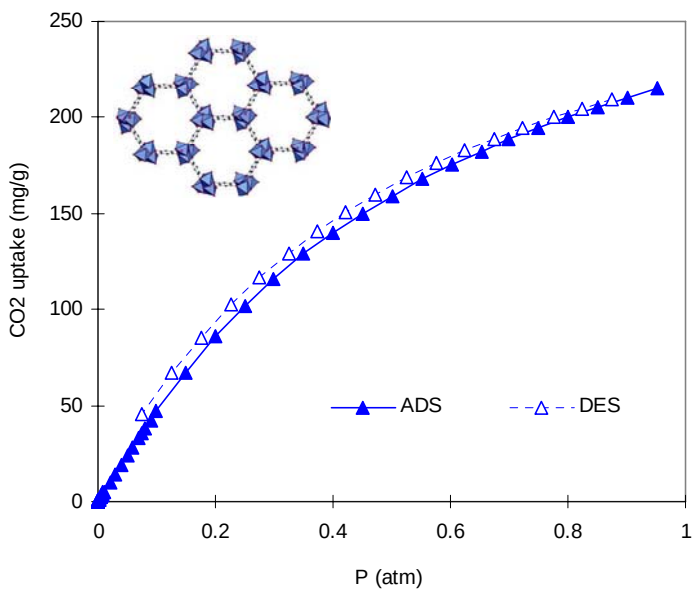

Figure 14. CO_2 adsorption isotherm at 298K for MOF-74. Inset shows MOF-74 structure.

4.2.5 Synthesis of MOFs with Mixed Linkers

The goal of producing a good MOF-based CO_2 sorbent in a cost effective manner is most likely going to be met by a using a relatively inexpensive organic linker with a common metal. The particular combination needed is, at least with the current understanding of MOF assembly, only possible to determine empirically. The traditional paradigm of synthesizing a new organic linker and testing against a panel of metals may lead to such a suitable material, but the choice of organic linker must be restricted to those readily available. This limits considerably the number porous solids that can be produced. Motivation by a desire for the synthesis of new MOFs from inexpensive precursors we hypothesized that a simple but potentially useful method for generating new structures would be the combination of multiple linkers with a metal. In the case of employing two different linkers possessing the same coordinating functionality, experimental data are lacking, and there is no basis for answering even the most basic question of phase composition. In broad terms we can expect two different behaviors in a crystalline mixed linker coordination polymer. The default behavior for two components combined and allowed to crystallize is segregation; this forms the basis of purification by crystallization. By contrast, the default behavior when monomers of similar reactivity are combined is random copolymerization. Therefore, it is interesting to contemplate whether in a porous crystal where strong bonds reversibly assemble the framework, copolymerization patterns will dominate or if self-sorting crystallization will prevail. If the former occurs this would represent an expeditious route to discover new porous solids. This approach allows for the construction of coordination polymers that are either isomorphic or non-isomorphic with respect to the MOFs derived from the pure linkers. The term “non-isomorphic” refers to materials which have substantially different network structure, whereas the term “isomorphic” refers to materials which have the same network structure.

4.2.5.1 Isomorphic Mixed Linker MOFs

If the two linkers employed are of similar geometry, such that the MOFs they produce are isostructural, we refer to this as the “isomorphic” mixed linker approach. An example for generating isomorphic materials is the combination of H_2BDC and functionalized H_2BDC linkers. In case of isomorphic materials, the feed ratio of the two linkers does not influence the underlying network structure of the product. For example, the products derived from feed ratios of 11:1 to 1:1 (mols H_2BDC:mols 2-aminodicarboxylic acid (H_2ABDC)) with 3 mols of zinc nitrate tetrahydrate in diethylformamide (DEF) have the same crystal structure as IRMOF-1 and IRMOF-3 (**Figure 15A**). In order to analyze the composition of the product, the materials were evacuated at room temperature for 2h to remove all solvent occluded in the pores of the compounds. The fully dried materials were decomposed in 1 M NaOH in D_2O solution. The decomposed samples were characterized by ^1H NMR. Peaks for both H_2BDC and H_2ABDC were well resolved allowing the quantification of each of the linkers in the final product. As shown in **Figure 15B**, the ratio of the linkers in the products determined by NMR agrees well with the initial feed ratio of the two linkers. As expected, increasing the concentration of ABDC, the BET surface areas decrease from that of H_2BDC and zinc nitrate tetrahydrate

(IRMOF-1, 2720 m^2/g) to that of H_2ABDC and zinc nitrate tetrahydrate (IRMOF-3, 2230 m^2/g) (**Figure 16A**). The CO_2 uptake of the products tracks similarly with the BET surface area (**Figure 16B**).

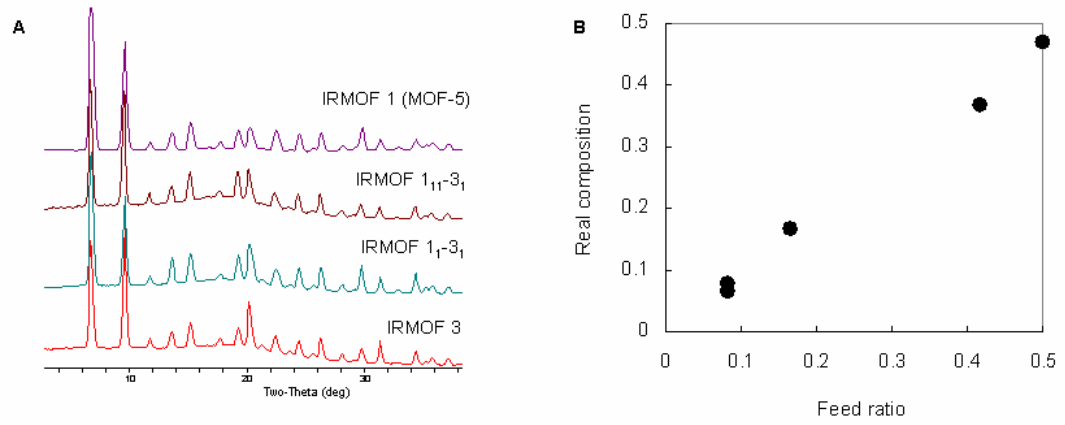

Figure 15. A. Powder XRD data for the products with different ratios of isomorphous linkers. **B.** Feed ratio (H_2BDC:H_2ABDC) vs. measured H_2BDC:H_2ABDC ratio in isomorphous MOFs.

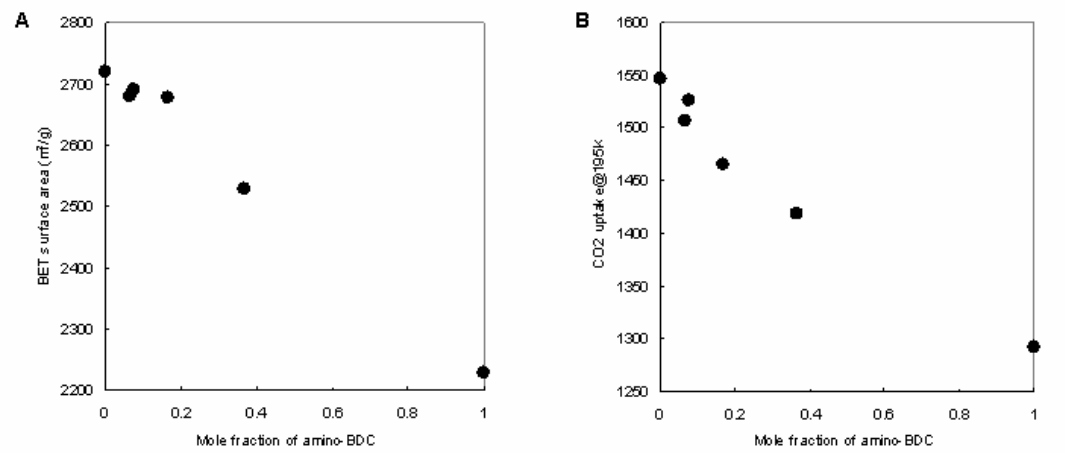

Figure 16. A. BET surface areas of isomorphic mixed MOFs as a function of ABDC:BDC mol ratio. **B.** CO_2 uptake at 195K of isomorphic mixed MOFs as a function of ABDC:BDC mol ratio.

4.2.5.2 Non-isomorphic Mixed Linker Coordination Polymers (MOFs)

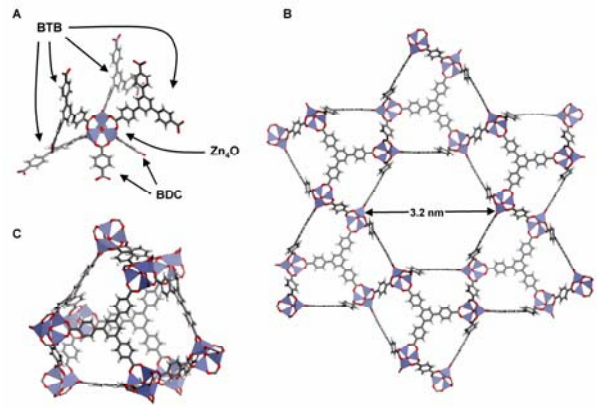

Figure 17. Structure of UMCM-1.

To illustrate the non-isomorphic approach consider the combination of H_2BDC and 1,3,5-tris(4-carboxyphenyl)benzene (H_3BTB). The crystal structure of IRMOF-1 shows it to be a simple cubic net in the *Fm*-3*m* space group[1g]. Similarly, pure H_3BTB reacts with zinc nitrate to produce MOF-177 which is in the trigonal $P3_1c$ space group[1d]. However, if H_2BDC and H_3BTB are mixed together in the presence of zinc nitrate, a new phase is formed. The product distribution can be controlled by the mole ratio of H_2BDC to H_3BTB. At a ratio of 3:2 (H_2BDC:H_3BTB) a single needle-shaped phase is obtained. A single crystal X-ray diffraction study of these needles revealed a 1D hexagonal channel structure. The product crystallizes in the hexagonal space group $P6_3/m$ and is non-isomorphic to the structures described above for the given pure linkers. The framework of the material consists of Zn_4O metal clusters linked together by two BDC and four BTB linkers arranged in an octahedral geometry (**Figure 17A**). The two BDC linkers are adjacent to each other leaving the other four positions occupied by BTB linkers. Analysis of the structure shows it has both micropores and mesopores. The micropores can be found in the cage-like structure formed by six BDC linkers, five BTB linkers, and nine Zn_4O metal clusters (**Figure 17C**). Six such microporous cages come together in an edge-sharing fashion to form one mesopore (**Figure 17B**). The product constructed with BDC and BTB linkers is denoted as UMCM-1 (University of Michigan Crystalline Material-1).

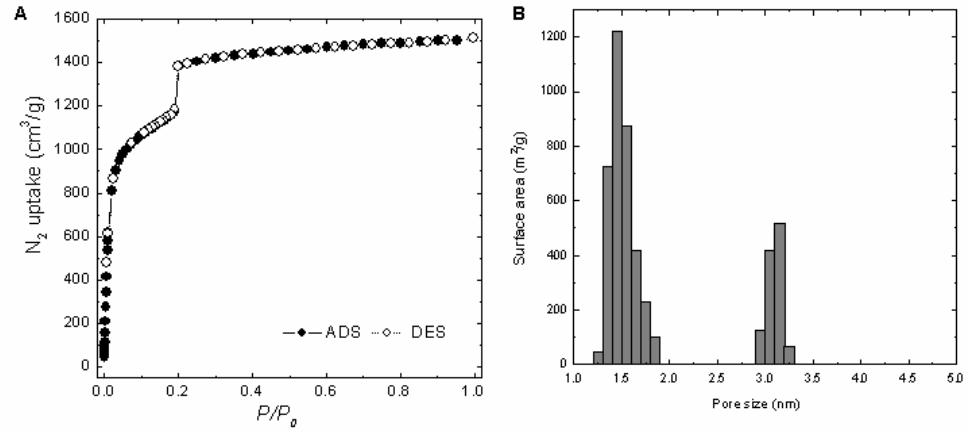

Figure 18. A. Nitrogen sorption isotherm at 77 K for UMCM-1 (●, adsorption; ○, desorption) **B.** Pore size distribution calculated after fitting DFT models to Argon gas adsorption data at 87 K.

The N_2 uptake data of UMCM-1 is shown in **Figure 18A**. The isotherm can be classified as a type IV isotherm[6], indicating that the UMCM-1 contains mesopores. The BET

surface area is 4160 m^2/g. Pore size distribution analysis by DFT methods utilizing Ar gas at liquid Ar temperatures reveals that there is a narrow distribution of micropores centered at about 1.4 nm and a narrow distribution of mesopores centered at about 3.1 nm (**Figure 18B**).

A second example of a non-isomorphic coordination polymer arises from the combination of thieno[3,2-b]thiophene-2,5-dicarboxylate (H_2T^2DC) and H_3BTB. At a feed ratio of 1:1 (H_2T^2DC:H_3BTB) a hexagonal plate-like phase is obtained. A single crystal X-ray diffraction study of these plates shows that the product crystallizes in the hexagonal space group $P6_3$. The framework of the material consists of Zn_4O metal clusters linked together by two T^2DCs and four BTBs arranged in an octahedral geometry. In this structure the T^2DC links are disposed both opposite to each other as

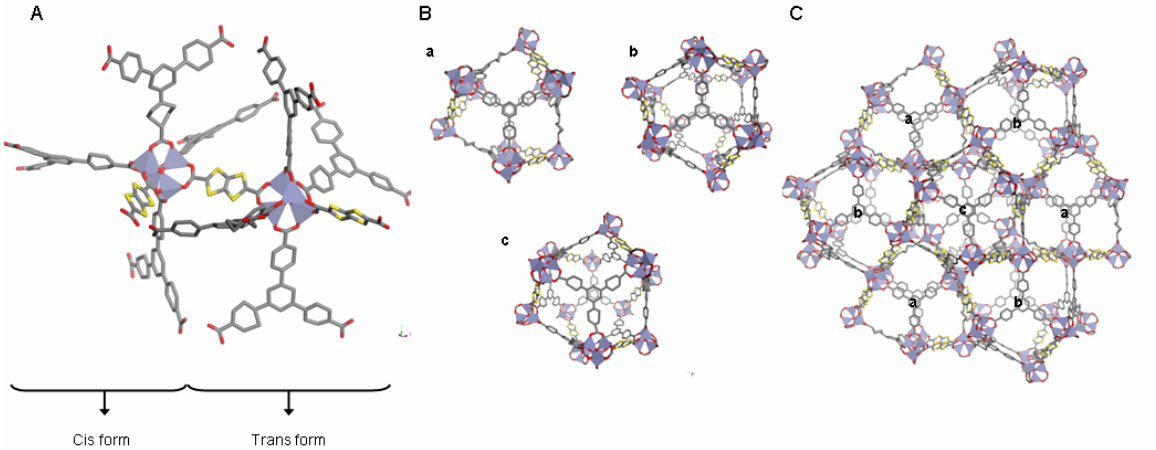

Figure 19. Crystal structure of UMCM-2. **A.** Zn4O units linked to six linkers **B.** Cages of UMCM-2. **C)** A view of UMCM-2 along the c-axis.

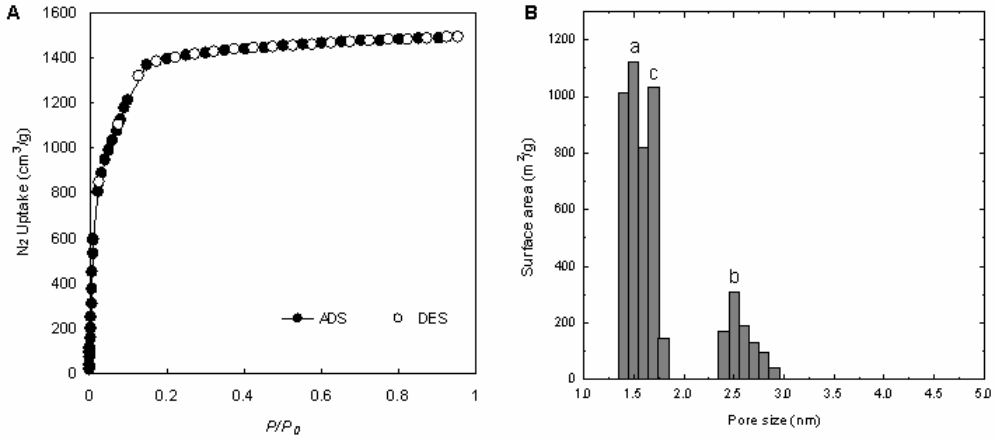

Figure 20. A. Nitrogen sorption isotherm at 77 K for UMCM-2 (●, adsorption; ○, desorption) **B**. Pore size distribution calculated after fitting DFT models to Argon gas adsorption data at 87 K.

well as adjacent to each other leaving the other four positions occupied by BTB linkers (**Figure 19A**). Analysis of the structure shows it consists of two different microporous cages (a and c in **Figure 19B**) and a mesoporous cage (b in **Figure 19B**). **Figure 19C** shows the assembly of these cages viewed along the c-axis where the central mesoporous cage b is surrounded by six alternating cages of a and c.

This material is denoted as UMCM-2. The N_2 uptake data of UMCM-2 shows that the isotherm can be classified as a type IV isotherm, indicating that the UMCM-2 contains mesopores (**Figure 20A**). The BET surface area is 4750 m^2/g. Pore size distribution analysis by DFT methods utilizing Ar gas at liquid Ar temperatures shows that there is a narrow distribution of micropores centered at 1.5 nm and 1.7 nm, and a narrow distribution of mesopores centered at 2.5 nm (**Figure 20B**).

Two other UMCM MOFs were prepared near the end of the project. UMCM-3 (**Figure 21**) was prepared from a zinc salt and a mixture of the benzenedibenzoic acid (BTB) linker utilized in UMCM-1 and UMCM-2 and thiophene dicarboxylic acid (TDC), while UMCM-4 (**Figure 22**) was prepared from zinc, BDC, and triphenylcarboxylic acid amine (TCA). Nitrogen adsorption results for both materials are provided as **Figure 23**. UMCM-3, composed of one medium-sized (TDC) and one large (BTB) linker, respectively, possesses a much higher surface area than UMCM-4, which is prepared from one small (BDC) and one large (TCA) linker, respectively. Other UMCM-3 and UMCM-4 properties were not available by the end of the project.

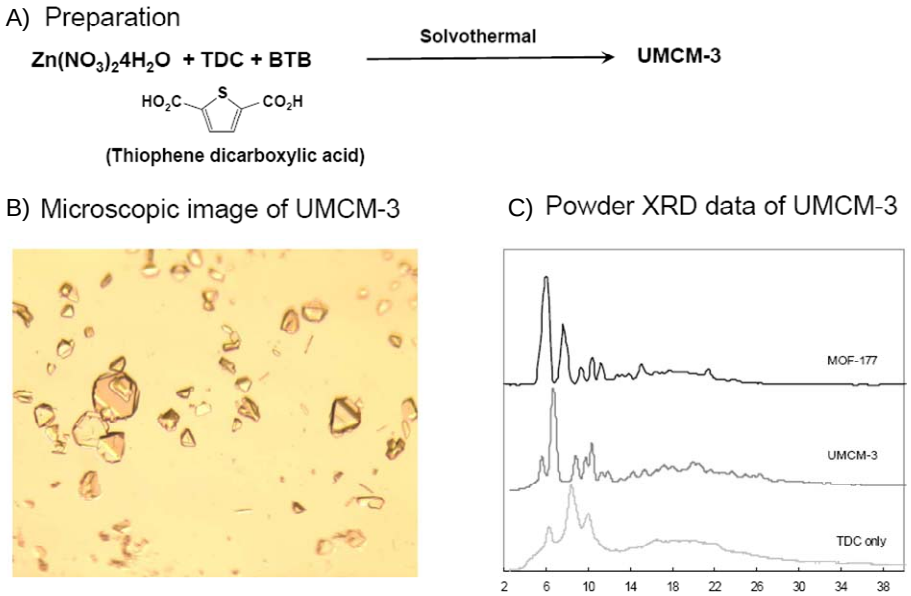

Figure 21. UMCM-3 details. A. Preparation. **B**. Optical microscopic image. **C.** Powder XRD patterns for UMCM-3, MOF-177 and TDC linker.

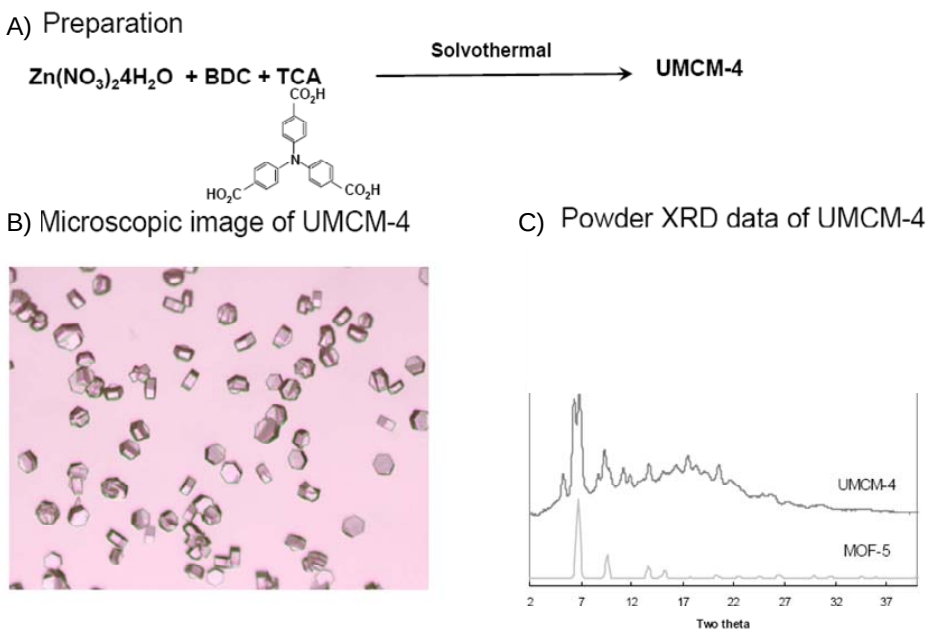

Figure 22. UMCM-4 details. A. Preparation. **B**. Optical microscopic image. **C.** Powder XRD patterns for UMCM-4 and MOF-5.

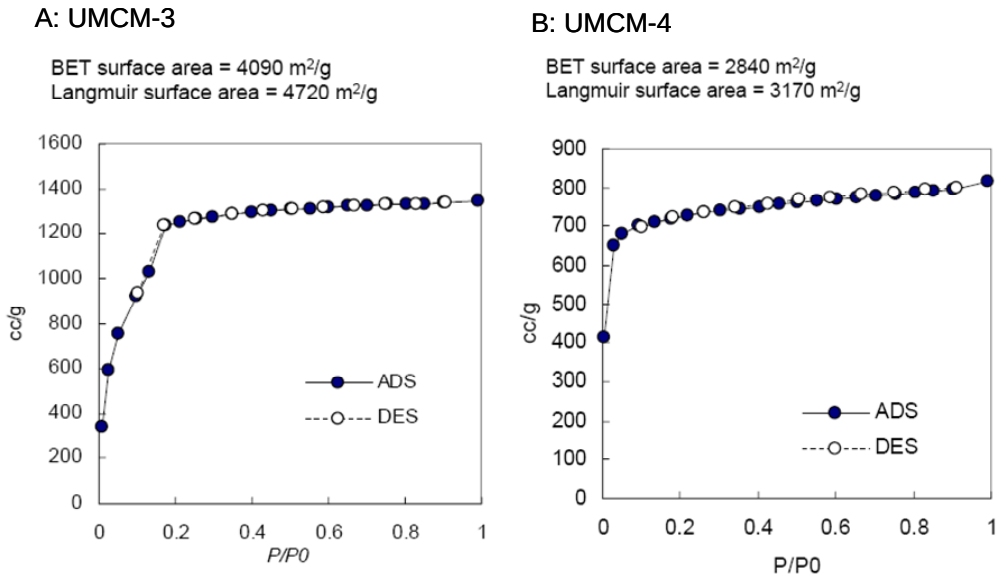

Figure 23. Nitrogen adsorption data for **A.** UMCM-3 and **B.** UMCM-4.

4.2.5.3 CO_2 Uptake of MOFs UMCM-1 and UMCM-2

Both UMCM-1 and UMCM-2 have high surface areas which are close or higher than the surface area of MOF-177. This implies that high CO_2 uptake via physisorption is possible in these compounds. As shown in **Figure 24**, the CO_2 uptake of both of UMCM-1 and UMCM-2 are close to that of MOF-177 and in fact are the three highest CO_2 capacity materials reported to date. An important finding in these materials is that for the CO_2 uptake of UMCM-2, a material that has a lower mesoporous contribution towards the surface area than UMCM-1, is greater than that of UMCM-1. This suggests that larger pores (mesopores) do not necessarily help to improve the CO_2 uptake capacity

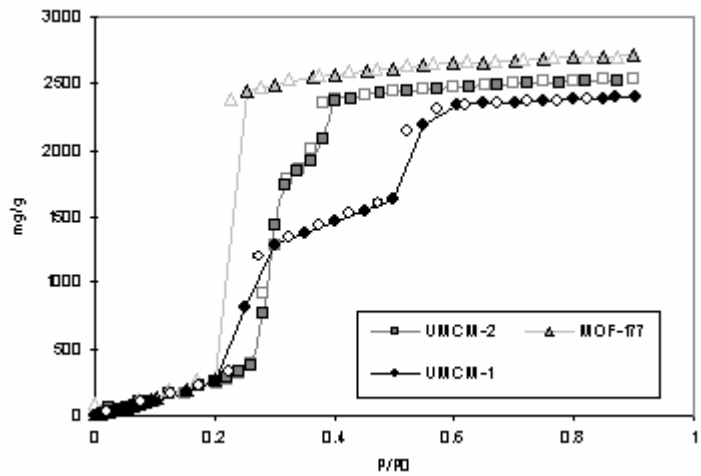

Figure 24. CO_2 sorption isotherm at 195 K for UMCM-1, UMCM-2, and MOF-177.

4.2.6 Scale-up and Forming of MOFs

Scale-up. Seven MOFs have been prepared in common industrial scale 2-liter (2L) reaction vessels. Yields and reproducibility have been good for five MOFs, including nano-IRMOF-1, Cu-BTC, and MIL-53. Based on past experience in zeolite and other inorganic and microporous materials commercial-scale synthesis, it is anticipated that further scale-up would be relatively straightforward for these MOFs.

Forming. Binding of MOFs, in particular Cu-BTC, was a challenge. Increasing the graphite as binder levels did not improve the ease of forming, nor did pre-drying at 170 ^{o}C overnight or wet dispersion in CH_2Cl_2 with drying at 100 ^{o}C. The effects of wet dispersion combined with centrifugation and drying before forming were investigated, but poor results were obtained. Near the end of the project, we switched to organic polymers as binders. Rubbery polymers worked well and thus would serve as a starting point for future forming studies in the second DOE/NETL sponsored programmed administered by UOP LLC (DE-FC26-07NT43092).

4.3 Molecular Modeling/ Virtual High-Throughput Screening

One of the objectives of this program was to develop molecular modeling techniques to predict isotherms for the components of flue gas and gasification streams on MOFs. The major components of these streams are CO_2, N_2, CH_4, H_2, and H_2O. Water is quite polar, and CO_2 and N_2 both have significant quadrupole moments. Therefore the interactions of the charge distribution of the MOFs and the sorbate molecules will have a significant impact on the selectivity and capacity for CO_2 and N_2.

4.3.1 General Molecular Modeling Considerations

The objectives during the first half of the project were to develop a model to calculate adsorption isotherms and heats of adsorption for CO_2 and other small molecules in MOFs, and to use the model to understand the inflection observed in experimental CO_2 adsorption isotherms in IRMOFs.

In the model that we developed, the MOFs and adsorbate molecules are represented in atomistic detail, placing Lennard-Jones sites and partial charges on all atoms. Careful selection of the sorbate/sorbate potential parameters is essential, and in previous work it was found that choosing a model that works well for vapor-liquid equilibria is a good strategy. Therefore Lennard-Jones parameters and partial charges from the TraPPE force field for CO_2, N_2, methane, and alkanes have been utilized.[7] Lennard-Jones parameters for the MOF atoms were taken from the DREIDING force field.[8] Previously we found that DREIDING worked well for predicting adsorption isotherms of methane and hydrogen in MOFs.[9,10] During the project, partial charges were calculated for the framework atoms of a variety of MOFs using density functional theory calculations on small pieces of the MOF structures.

To test the model, adsorption isotherms for CO_2 were calculated for a set of test cases using grand canonical Monte Carlo (GCMC) simulations.[11] As shown in **Figure 25**, the predicted CO_2 isotherms match quite well with the experimental isotherms for IRMOF-1, IRMOF-3, and IRMOF-6. Results also matched experiment well for MOF-177 (not shown). In addition, the simulations capture the complex temperature dependence of the isotherms essentially quantitatively, as shown in **Figure 26**. Electrostatic interactions were found to be crucial to reproduce the inflections and steps observed in the isotherms. (See **Figure 25a.**)

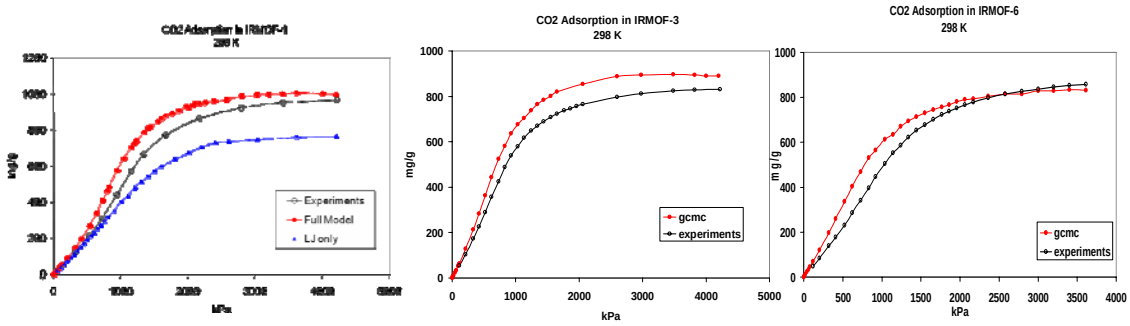

Figure 25. Comparison of simulated and experimental adsorption isotherms for CO_2 at 298 K in a) IRMOF-1, b) IRMOF-3, and c) IRMOF-6. *For IRMOF-1, the isotherm in blue includes only Lennard-Jones interactions. The simulation with only Lennard-Jones interactions does not capture the the inflection observed in the experimental isotherm, but the full model (in red) that also includes the Coulombic interactions successfully captures the shape of the isotherm.*

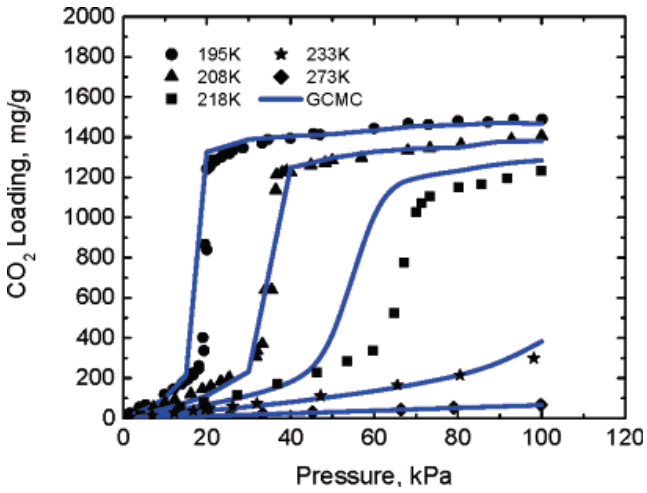

Figure 26. Comparison of simulated and experimental adsorption isotherms for CO_2 in IRMOF-1 at various temperatures.

To study the effect of linker functionality on CO_2 adsorption, isotherms in IRMOF-1, 3, and 6 are compared in **Figure 27**. IRMOF-1 has a benzenedicarboxylate linker with no functional groups attached, whereas IRMOF-3 and IRMOF-6 have amino and alkyl functionalized linkers, respectively. IRMOF-1 has the highest saturation capacity and

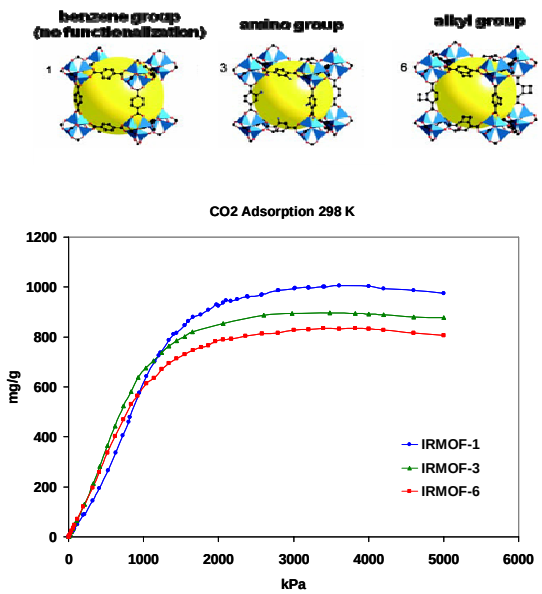

Figure 27. Comparison of simulated adsorption isotherms for CO_2 in IRMOFs-1, -3, and -6 at 298 K.

IRMOF-6 has the lowest. These results can be explained on the basis of the free volume of the frameworks. IRMOFs-3 and -6 have reduced pore volumes due to the amine and cyclobutane groups that protrude into the cavities. These groups, however, promote adsorption at low pressures, where IRMOF-3 and IRMOF-6 show higher adsorption than IRMOF-1.

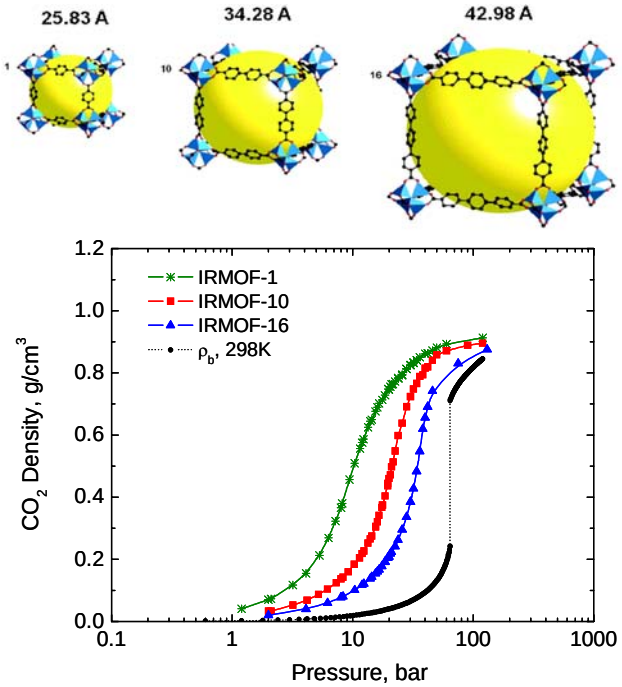

Figure 28. Density of CO_2 in IRMOF-1, -10, and -16 compared with bulk values at 298 K. The adsorbed phase densities are calculated considering only the free volumes of the crystal structures.

Analysis of the CO_2 positions in the simulations reveals that below the sharp rise in the isotherms of **Figure 26**, molecules are mostly adsorbed near the corners of the MOF cavities. With increasing pressure, the pores fill, leading to a type V isotherm. Type V isotherms are relatively rare and are often accompanied by hysteresis. However, neither the experiments nor the simulations display hysteresis. To shed more light on the pore filling, we plotted the density of CO_2 within the pore volume of IRMOFs-1, -10, and -16 at 298 K (**Figure 28**). IRMOF-10 and IRMOF-16 possess approximately double and triple the pore volume per gram of IRMOF-1. The bulk density of CO_2 is also shown in the figure. From these results, we find that the pressure of the pore filling shifts toward the bulk condensation pressure with increasing pore size (IRMOFs-1, -10, -16).

Molecular simulations of mixtures were also performed. Predicted results for equimolar mixtures of CO_2/CH_4 and CO_2/N_2 in IRMOF-1 are shown in **Figure 29**. For the CO_2/CH_4 mixtures, methane adsorption is significantly suppressed by the presence of the more strongly adsorbed CO_2 compared to single-component adsorption at the same (partial) pressures. This effect is also seen for nitrogen to a lesser extent.

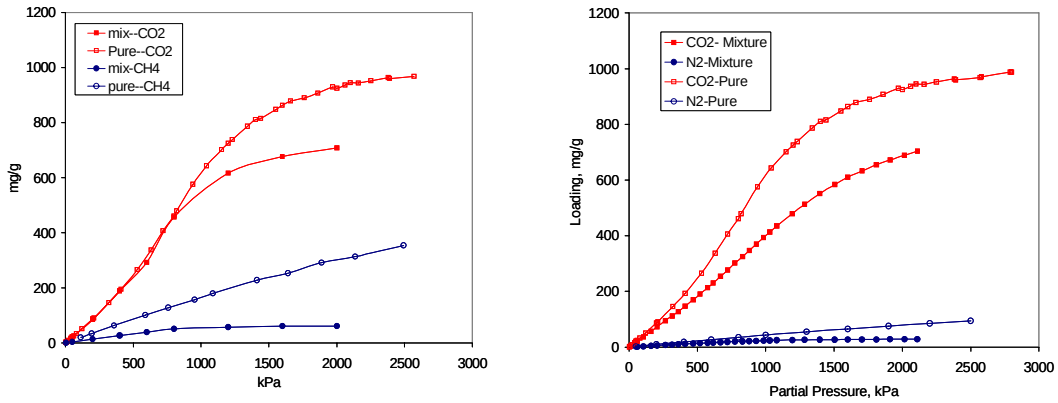

Figure 29. Adsorption of equimolar mixtures of a) CO_2/CH_4 and b) CO_2/N_2 in IRMOF-1 at 298 K as predicted by GCMC simulation. Pure component results are also shown for comparison.

More recent objectives have been to

- Use the model to evaluate MOFs for separations involving CO_2.
- Predict maximum expected surface areas for wide variety of MOFs from our project and the open literature.

Therefore, in the next phase of the project, we investigated MOFs with a wider range of framework topologies and other characteristics. The MOFs of interest included IRMOF-20,[5] Cu-BTC,[12] MOF-11,[13] Dy-BTC,[14] and Pd-2-pymo.[15] Based on our previous success, we used the same basic models to simulate the adsorption isotherms for CO_2, CH_4, N_2, and H_2 in these MOFs. First, we addressed a few technical details using Cu-BTC as a test case. For example, a question about the correct C-H bond lengths in MOFs was answered. Crystal structure data reported for MOFs usually include unusually short C-H

bond lengths, 0.93 Å in CuBTC, for instance. Note that the hydrogen atoms are not generally observable in x-ray diffraction, and the positions reported are generated by the crystallographers. Optimizing this bond length using quantum mechanical calculations results in a more reasonable value of 1.093 Å. However, simulated CO_2 isotherms with the two different C-H bond lengths did not show significant differences, indicating that it is OK to use the values reported in the MOF crystal structures.

4.3.2 MOF Surface Areas

A key characteristic for MOFs is high surface area. Occasionally, authors report surface area values that are lower (or higher) than what one should expect for a given MOF

Table 2. Calculated surface areas for several key MOFs.

Material	Crystal density	Surface Area				Free Volume (0 Å probe)	
		Hydrogen Probe (2.958 Å)		Nitrogen Probe (4.54 Å)			
		SA / mass (m^2 / gr)	SA / volume (m^2 / ml)	SA / mass (m^2 / gr)	SA / volume (m^2 / ml)	Void fraction	FV / mass (ml / gr)
IRMOF-1	0.593	3891.7	2307.8	3192.2	1893.0	0.783	1.319
IRMOF-3	0.634	3679.8	2333.0	2887.8	1830.9	0.764	1.204
IRMOF-20	0.511	4021.1	2054.8	3648.9	1864.6	0.825	1.614
CuBTC	0.879	2598.3	2283.9	1542.8	1755.1	0.704	0.801
IRMOF-16	0.205	6051.1	1240.5	6314.8	1294.5	0.905	4.409
MOF-177	0.427	4924.9	2102.9	4627.9	1976.1	0.806	1.890
UMCM-1	0.338	5123.2	1731.6	4775.7	1614.2	0.837	2.146
MIL-101	0.327	4450.5	1455.3	3725.8	1218.3	0.824	2.517

structure. As such, we decided to calculate the expected highest possible surface area for several important MOFs[16]. Most match experimentally determined values closely (**Table 2**). Note that UMCM-1 has the highest calculated surface area MOF material to date. Recall that IRMOF-16 has not been synthesized – it is a hypothesized MOF only.

Table 3. Crystal density and surface areas for selected MOFs.

Material	crystal density, g/cc	calculated* surface area, (sq m/g)	measured** surface area (sq m/g)	reported surface area (sq m/g)
IRMOF-1	0.593	3563	3000	up to 4170
MIL-101	0.327	3725	2334	4100 to 5900
MOF-177	0.427	4833	4500	4500
UMCM-1	0.338	4972	4730	4730

***by Snurr, et al; ** BET method, measured at UOP or U Michigan**

Because these values represent the theoretical maximum surface area value for a given MOF, they serve as a nice benchmark for the experimental chemist. For example, **Table 3** lists the calculated maximum surface area for selected MOFs versus what we have measured and what has been reported. A graphical representation of our measured versus the calculated maximum values is provided as **Figure 30**. As can be seen in **Table 3**, some of the reported values (e.g., for MIL-101) don't make sense because the observed are larger than the theoretical maximum.

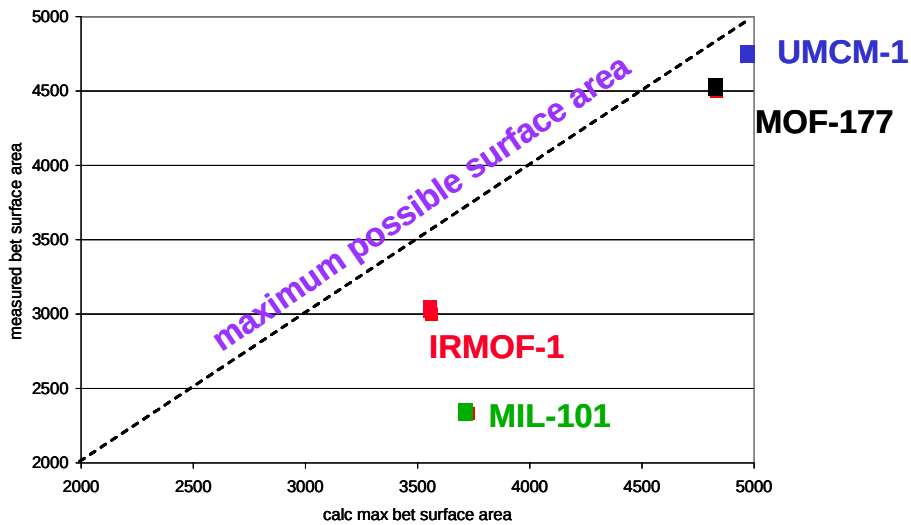

Figure 30. Measured (by our team) versus calculated theoretical maximum surface area for IRMOF-1, MIL-101, MOF-177 and UMCM-1.

4.3.3 Virtual High-Throughput Screening

Adsorption isotherms for CO_2, N_2, CH_4, and H_2 were calculated in the new MOFs at room temperature for screening purposes. The simulations predict the following order for single-component adsorption:

$$CO_2 > CH_4 > N_2 > H_2$$

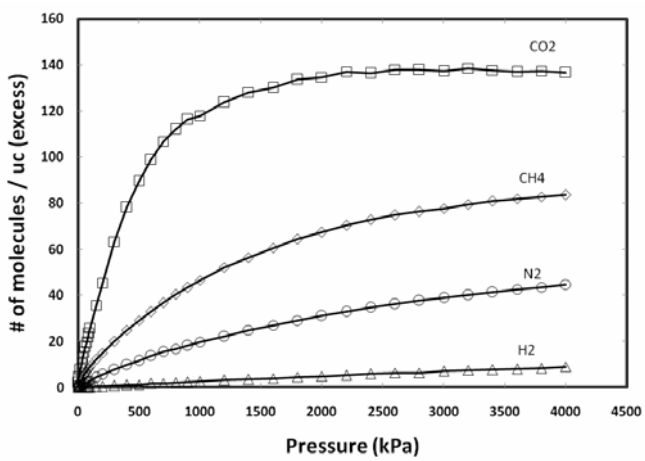

Figure 31. Comparison of simulated adsorption isotherms in CuBTC at 298K.

This correlates with the boiling points of the gases. Representative results for CuBTC are shown in **Figure 31**.

The following MOFs were chosen to investigate their performance for CO_2 separations at 298 K: Cu-BTC, Dy-BTC, Pd-2-pymo, IRMOF-20, and MOF-11. It should be noted that these MOFs represent a wide range of structures. This stands in contrast to the IRMOFs previously investigated, which all have the same basic topology and pore structure.

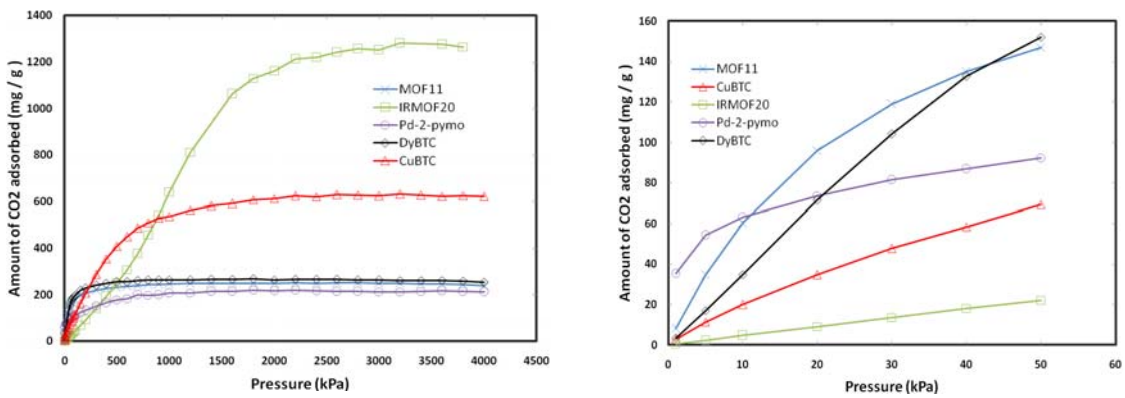

Figure 32. Comparison of simulated CO_2 isotherms at 298 K in five different MOFs for a) full pressure scale and b) low pressure region.

Comparisons of simulated CO_2 isotherms for several MOFs investigated are given in **Figure 32**. These results revealed that while MOFs with relatively large pores have higher saturation loading capacity, it is the MOFs with smaller pores that show promising performance to separate CO_2 from other gases at low pressures. MOF-11 is the only material where this order does not hold, as the amount of CO_2 and N_2 adsorbed is almost same. The likely explanation for this exception is that MOF-11 has two types of pores, and the larger pores adsorb both N_2 and CO_2 whereas the smaller pores only adsorb N_2.

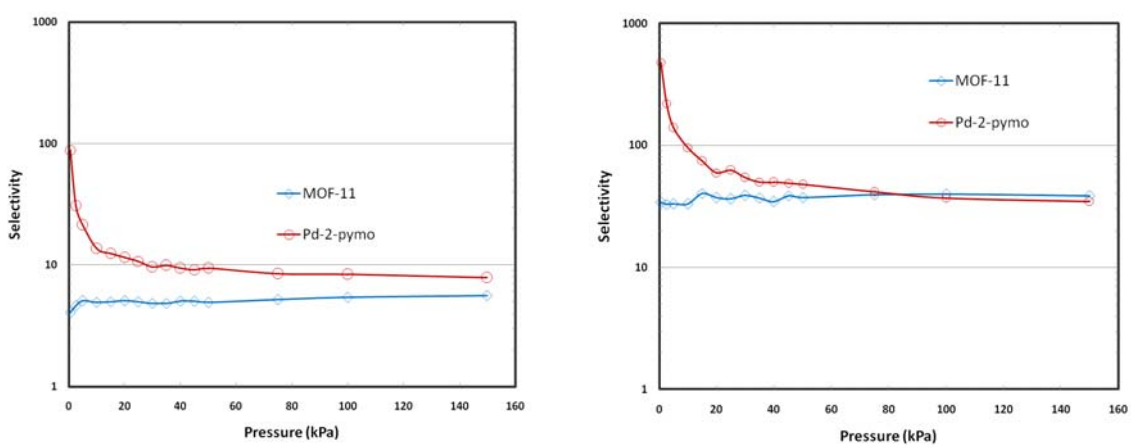

Figure 33. Comparison of selectivities of CO_2 at 298 K in Pd-2-pymo and MOF-11 for equimolar mixture of a) CO_2/CH_4 and b) CO_2/N_2.

At low pressures, Pd-2-pymo and MOF-11 are the most promising candidates for CO_2 separation among the MOFs investigated. Therefore, for these two MOFs equimolar mixture simulations of CO_2/CH_4 and CO_2/N_2 were performed. Predicted selectivities are shown in **Figure 33**. Pd-2-pymo shows a clear advantage over MOF-11 in terms of selectivity of CO_2 over CH_4 and N_2, but both MOFs show promising selectivities. A typical flue gas composition is around 10% CO_2, which implies a partial pressure of 10 kPa.

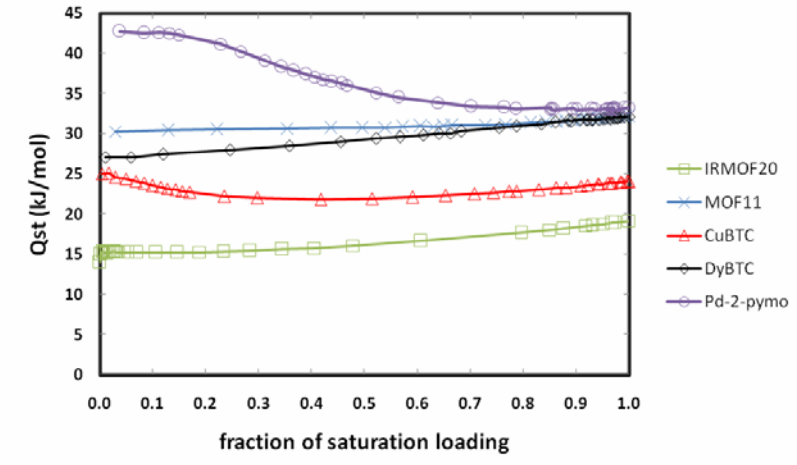

Figure 34. Comparison of simulated CO_2 heats of adsorption in give different MOFs at 298 K.

Heats of adsorption were also calculated from the simulations of CO_2 adsorption (see **Figure 34**). An overall comparison of the simulated CO_2 data suggests that several MOFs are promising in terms of CO_2 adsorption and high heat of adsorption (up to 35 kJ/mol) at low pressures.

4.3.4 Modeling Hydrolysis

Hydrothermal stability is an important property of a sorbent in a commercial process. It is difficult to rigorously exclude water from a commercial feed. Damage caused to a sorbent by exposure of moisture at process condition will limit the usefulness of the sorbent. It is also desirable to regenerate a sorbent after exposure to moisture. One would like to have a hydrothermally stable material which will not decompose when heated in the presence of moisture. A qualitative model was developed to predict the hydrothermal stability for MOFs. The primary purpose of this model is to predict the relative hydrothermal stability of MOFs, rather than predicting exactly the hydrothermal conditions at which a material would decompose. The understanding gained from this modeling effort would aid in the selection and design of hydrothermally MOFs. The calculations involved in this model should take less time and effort than experimentally synthesizing and testing the material.

Molecular dynamics simulations of IRMOF-1 predicted that metal organic frameworks are unstable above 4 wt% water.[17] Although these calculations are consistent with the observed hydrothermal instability of IRMOF-1 experimentally, they are not very realistic

models of the interaction of water with metal oxides. The force-field approach used in these simulations do not allow for the dissociation of water molecules. Therefore this simulation only includes hydration and not hydrolysis reactions in the model. The end product of the reaction of water with the metal oxide clusters in IRMOF-1 must include hydrolysis to some extent. The second issue with molecular dynamics with force-fields is that parameters needed to model the interaction of oxygen with other metals are not readily available. This will make it difficult to extend these calculations to MOFs containing other metals. This will be especially true for transition metals which are difficult to model with forcefields. Thirdly, the Zn-O parameters in this model are biased towards tetrahedral coordination of Zn by oxygen. Zn is known to have octahedral coordination in many compounds. Octahedral coordination of Zn by water and ligands will be important in modeling MOFs containing octahedral Zn and intermediates in the reaction of water with the metal oxide clusters. We have decided to use quantum mechanics to model the reaction of water with metal organic frameworks. Quantum mechanics does not require parameters for every metal ligand pair and can model hydrolysis reactions which involve the breaking of O-H bonds.

Unfortunately quantum mechanics requires orders of magnitude more computational effort than force-field calculations. The unit cells of metal organic framework can be very large (greater than 1000 $Å^3$). A quantum mechanical calculation of reactions in a unit cell of over 1000 $Å^3$ is not practical. MOFs are often amenable to cluster studies, however, since much of the organic ligand is not directly involved in the reaction between water and metal oxide clusters. Although one might expect the organic linkages between metal oxide clusters in MOFs to impose geometric constrains on the hydration and hydrolysis reactions, we have found that the bonds between the carboxylate groups and metals can bend perpendicular to the plane formed by the carboxylate group. The metal-ligand ligand bonds act like a hinge which allow ligands to move fairly easily during reactions with water.

For example, the ligand displacement reaction involves a water molecule starting near the inorganic fragment of the MOF and inserting into one of the metal ligand bonds of the inorganic fragment. This reaction is shown in **Figure 20** for the displacement of the carboxylate ligand by water in IRMOF-1.

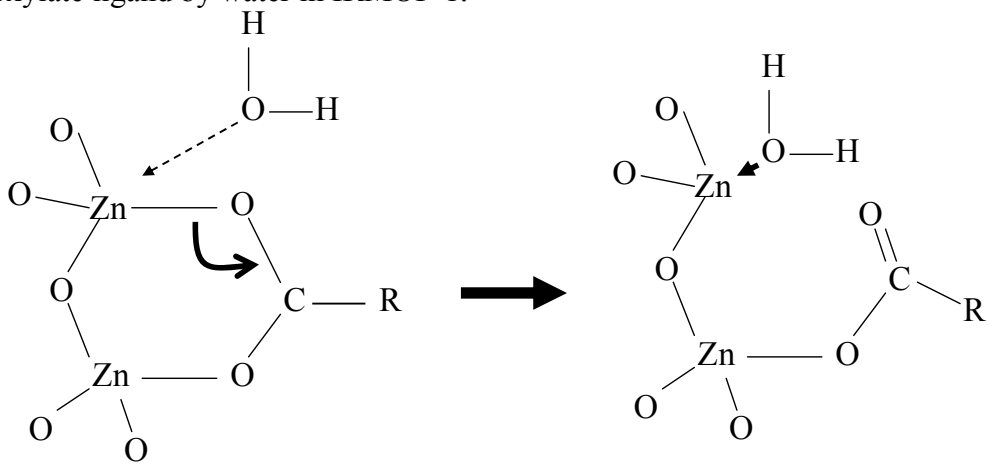

Figure 35. Proposed ligand displacement in IRMOF hydrolysis reaction.

In the reaction in **Figure 35**, a water molecule in the face of the tetrahedron of oxygen around Zn in IRMOF-1 pushes one of the carboxylate ligands out the coordination sphere of one the zinc atoms. The displaced carboxylate ligand, which started bridging two Zn atoms in the IRMOF-1 structure ends up coordinated to one Zn ligand.

A test of the approach described above is to compare the predicted energies of hydration and hydrolysis for three different MOFs with their observed hydrothermal stability. The program DMOL3 was used in this simulation.[18] The metal-oxide acetate clusters $Zn_4O(O_2CCH_3)_4$, $Cu_2(O_2CCH_3)_4$ and $Cr_3O(CO_2CH_3)_6F$ were used as models of the metal oxide clusters in IRMOF-1, HKUST-1 and MIL-101 respectively. Our experimental work has shown that IRMOF-1 is less stable than HKUST-1 and HKUST-1 is less stable than MIL-101. Two water molecules were added to the cluster models of $Cu_2(O_2CCH_3)_4$ and $Cr_3O(CO_2CH_3)_6F$ to complete the octahedral coordination of the metal atoms before the hydrolysis or hydration reactions. Two waters were added to $Zn_4O(O_2CCH_3)_4$ to allow octahedral coordination of a Zn atom during the hydration or hydrolysis reactions. The reaction of two molecules with $Zn_4O(O_2CCH_3)_4$ to form octahedrally coordinated Zn atoms is generally exothermic in IRMOF-1 and a precursor to low energy pathways to hydration and hydrolysis. The hydrolysis reaction is the reaction of two water molecules with an acetate ligand in the cluster complex to yield an acetic acid and a new cluster complex where a hydroxide anion and a water molecule is bonded to the coordination sites exposed by removal an acetate ligand. The hydration reaction is the reaction involves a water molecule, in the second coordination sphere of the metal atom, displacing a ligand from one of the metal atoms in the cluster and moving into the vacant coordination site vacated by the ligand. A schematic for the ligand displacement reaction is shown in **Figure 36**.

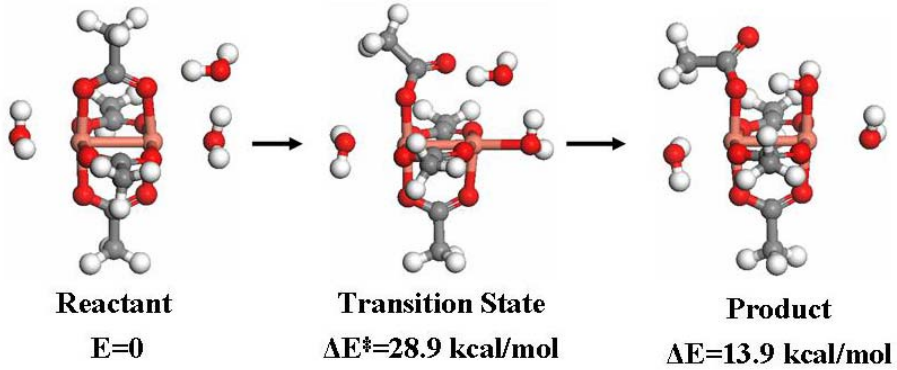

Figure 36. Ligand displacement reaction for $Cu_2(O_2CH_3)_4(H_2O) + H_2O$.

The predicted energies for hydrolysis and hydration are shown in **Table 4**. Note that the predicted energies for hydrolysis are in the reverse order from the observed hydrothermal stability. The predicted energies for hydration are in better agreement with observed hydrothermal stabilities. However the predicted activation energy for hydration

correlates with the observed hydrothermal stabilities of IRMOF-1, HKUST-1 and MIL-101.

Table 4. Reaction and Activation Energies (kcal/mol) Predicted for Reactions of Water with Cluster Models of MOFs.

Complex	MOF	Hydrolysis ΔE	Hydration ΔE	Hydration ΔE‡
$Zn_4O(O_2CCH_3)_6$	IRMOF-n	-7.3	0.1	11.6
$Cu_2(O_2CCH_3)_4(H_2O)_2$	HKUST-1	-8.8	13.9	28.9
$Cr_3O(O_2CCH_3)_6F(H_2O)_2$	MIL-101	-26.9	7.9	35.8

Since the hydration reaction modeled here involved the displacement of an acetate ligand from a Zn atom by water we will refer to this reaction as a ligand displacement reaction for the rest of this report. A scan of activation energies for ligand displacement reactions have been carried out for cluster models of several MOFs to help select hydrothermally stable MOFs for experimental characterization. The results of this scan are shown in **Table 5**. The metal organic frameworks which are built of infinite rods of metal oxides were modeled as 1-D infinite chains.

Table 5. Reaction Energies and Activation Energies (kcal/mol) Predicted for the Reaction of Water with Cluster Models of MOFs.

Complex	MOF	ΔE	ΔE‡
$Zn_4O(O_2CCH_3)_6$	IRMOF-n	0.1	11.6
$Zn_2(O_2CH_3)_4(C_5H_5N)_2$	MOF-508a	1.4	18.9
$Cu_2(O_2CCH_3)_4(H_2O)_2$	HKUST-1	13.9	28.9
$[Cr(OH)(O_2CCH_3)_2]_n$*	MIL-53	7.5	30.5
$Cr_3O(O_2CCH_3)_6F(H_2O)_2$	MIL-101	7.9	35.8
$Al_3O(O_2CCH_3)_6F(H_2O)_2$	Al-MIL-101	5.6	38.7
$[Zn_6(C_6H_4O(CO_2)_6(H_2O)_7]_n$*	Zn-MOF-74	3.5	42.0
$[Al(OH)(O_2CCH_3)_2]_n$*	Al-MIL-53	7.7	43.4
$Pd(C_4H_3N_2O)_2$**	Pd-pymo	78.3	79.6

*indicates that the model is actually an infinite 1-D chain.
** indicates that the model is actually the full crystal and not a cluster.

When these results are compared to the available experimental results a good correlation with experiment is observed. The discrepancies are most likely due to the neglect of the framework in the model. Since MIL-53 is observed to change lattice constants significantly when guest molecules are removed it is likely to be much more flexible than

MIL-101. The increased flexibility of MIL-53 framework makes it less stable than would be expected based activation energies calculated for clusters which neglect the framework.

Valuable qualitative insights can be gleaned from the activation energies for ligand displacement on cluster complexes. Note that when comparing MOFs containing different metal with similar ligands, MOFs made with metals with stronger metal oxygen bonds tend to be more stable. For example the metal oxygen bond strengths for Zn, Cu, Cr and Al are 365, 371, 446 and 514 kJ/mol respectively. These bond strengths parallel the hydrothermal stability of the MOFs bridged by carboxylate ligands. For example the IRMOF series is less stable than HKUST-1 (Cu-BTC) and the Al and Cr containing MOFs in the MIL-101 and MIL-96 are more stable than the IRMOFs or HKUST-1. Stronger metal oxide bonds will tend to be more hydrothermally stable, because the activation energy for ligand displacement will be higher for ligands with larger metal-ligand bonds. Metal organic frameworks constructed from metal clusters linked by carboxylate ligands tend to be more stable if they contain octahedrally coordinated metal ions than tetrahedral coordinated metal ions. For example, the IRMOF series is less stable than MOF-74. This trend should hold for other bridging ligands, as well. However, it will hold only when comparing MOFs with similar ligands and metals. Note that MOFs bridged by η-2 carboxylate ligands will tend to have hydrothermal stability issues because it is relatively easy to displace a η-2 carboxylate ligand by changing it to η-1 and adding a ligand to the open coordination site.

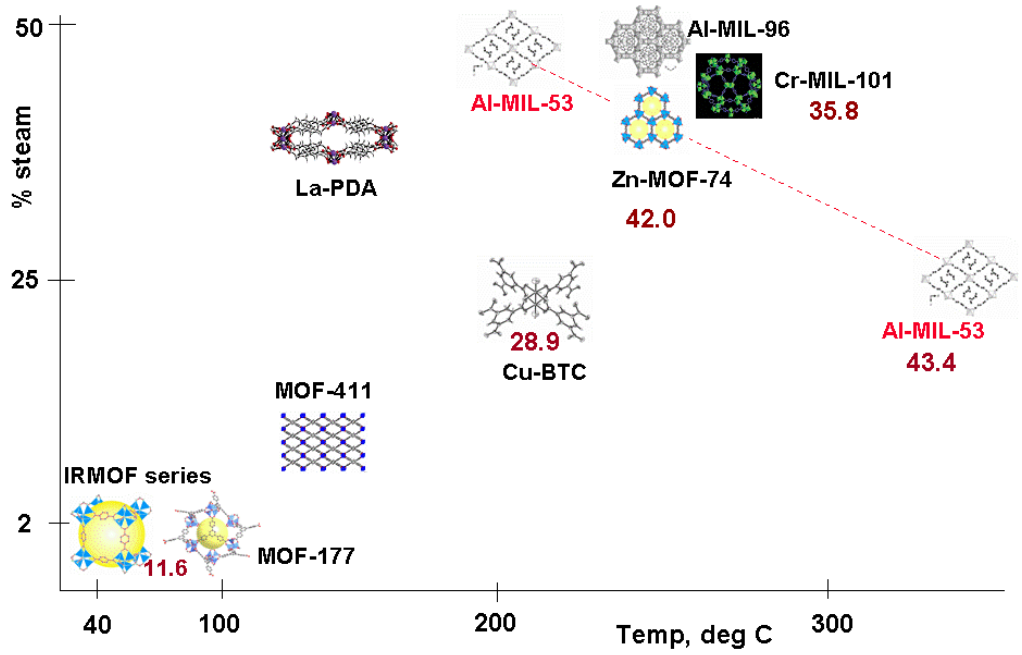

Figure 37. Steam stability map. Map locations are experimentally determined, and maroon numbers are calculated ligand replacement reaction activation energies in kJ/mol.

The cluster model presented here does yield qualitatively correct trends in hydrothermal stability. This indicates that the strength of the bond between the metal oxide cluster and the bridging ligand is important in determining the hydrothermal stability of the MOF. Although the flexibility of the framework plays a role, it is not as important as the metal-ligand bond strength. The trends predicted by the model yields simple concepts which can be used to select and invent hydrothermally stable MOFs.

4.4 Hydrothermal and Other Contaminant Stability

Another focus of the project was the thermal and oxidative stability of MOFs. In particular the hydrothermal stability and contaminant sensitivity of MOFs was evaluated. The results of the stability studies will be taken into account when flow schemes are developed for the incorporation of MOFs into flue gas and gasification streams. For

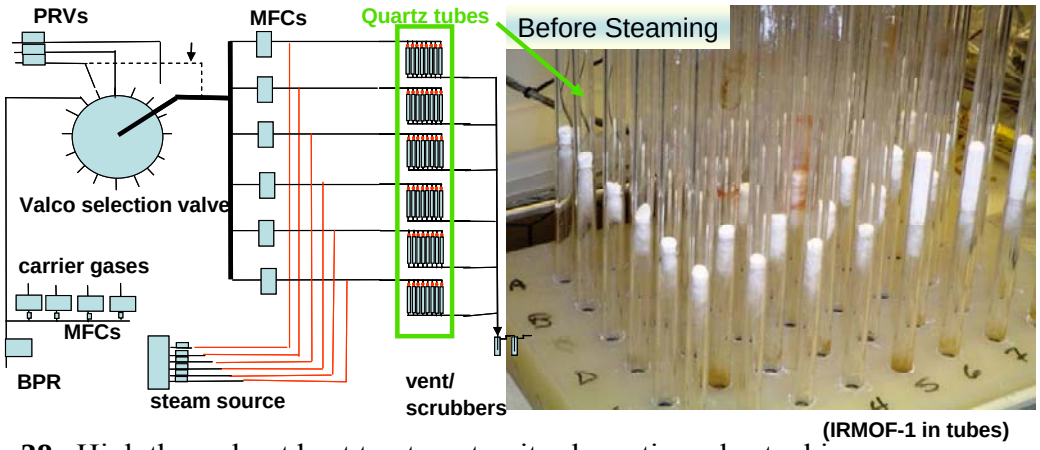

Figure 38. High throughput heat treatment unit schematic and actual image.

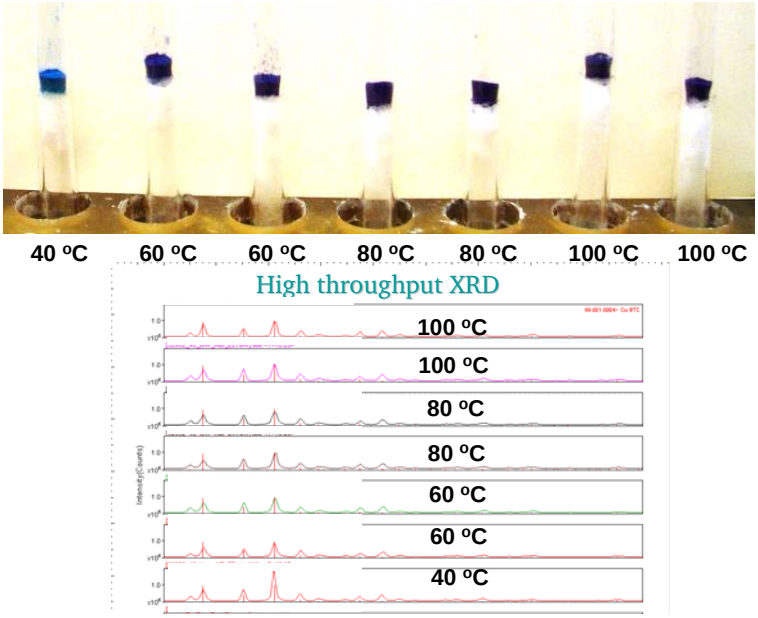

Figure 39. **A**. Cu-BTC in quartz tubes after steaming. **B**. XRD results for these samples.

example, if MOFs exhibit limited stability in the presence of contaminants, a guard bed will be incorporated into the flow scheme to remove the contaminant. For flue gas streams the primary contaminants are SO_x, NO_x and water. Typical contaminants present in IGCC/ gasification streams are acid gases such as H_2S and COS. The thermal stability of MOFs will determine the final operating temperature of the CO_2 capture process.

As an example, a hydrothermal stability experiment was conducted on Cu-BTC. The high-throughput heat treatment unit (HTU) is configured in a 6 row by 8 column format (**Figure 38**). After activation at 200 ^oC, the samples were cooled in dry air, then subjected to 0 to 7 mole% steam at temperatures from 40 to 100 ^oC. After heat treatment, samples were cooled in dry air and then analyzed by high-throughput powder X-ray diffraction analysis (XRD). Example results (shown in **Figure 39**) suggest that the Cu-BTC structure is maintained at all steam levels at 100 ^oC.

MOF-74 and Cu-BTC were subjected to severe steaming – up to 350 ^oC and 50 mole% steam (**Figure 40**). For MOF-74, at a fixed temperature, crystallinity decreases with increasing steam level, and at a fixed steam level, crystallinity did not change with increasing temperature up to 300 ^oC. The sample decomposed between 300 – 350 ^oC. For Cu-BTC, at temperatures 250 ^oC and above, crystallinity disappeared at 35+ % steam. At a fixed steam level, crystallinity did not change with increasing temperature up to 250 ^oC at 25% steam and up to 200 ^oC at 35+ % steam. Cu-BTC decomposed at 250 – 300 ^oC at 25% steam and at 200 – 250 ^oC at 35% steam.

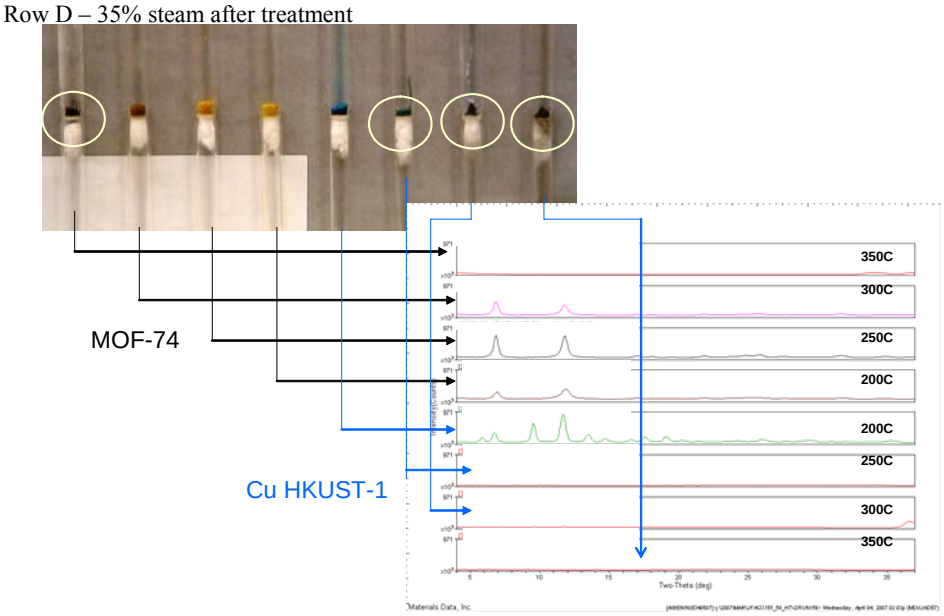

Figure 40. A) MOF-74 and Cu-BTC (a.k.a., HKUST-1) in quartz tubes after heat treatment. B) XRD results for these samples.

An Al-containing MOF, MIL-53, prepared based upon literature reports, is among the most moisture-stable MOF evaluated to date. Example XRD data obtained after hydrothermal treatment at various conditions is provided as **Figure 41**.

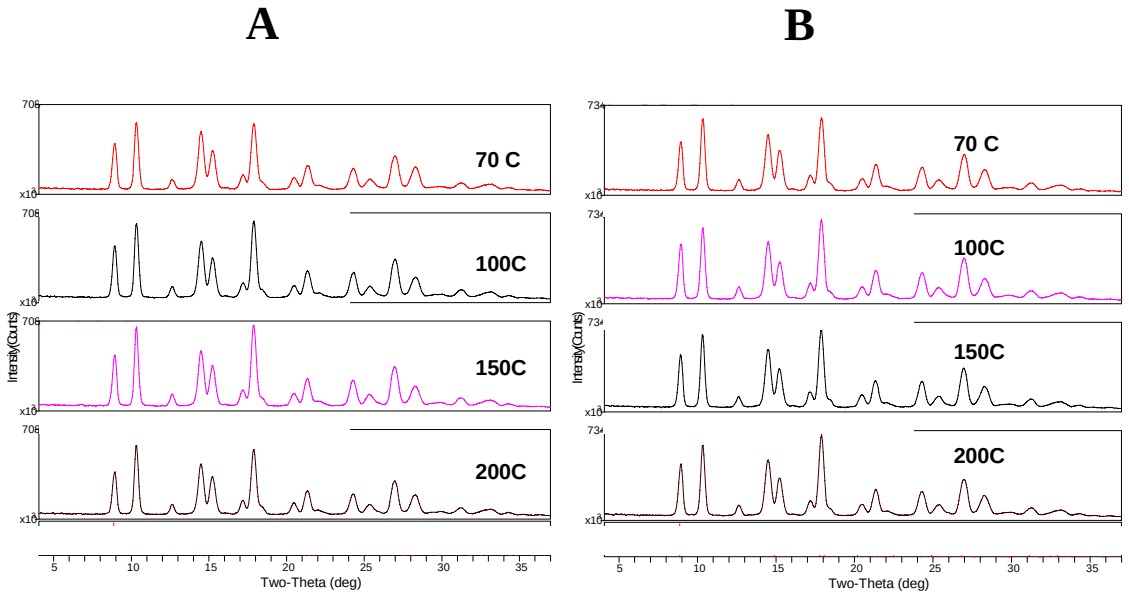

Figure 41. XRD results on MIL-53 showing that structural integrity is maintained at all conditions shown. **A** 25 mol% steam. **B** 50 mol% steam

Subsequently, samples of MIL-53 and MIL-96 were subjected to very severe steaming – up to 450 ^{o}C and 50 mole% steam. Both samples maintained XRD structure until 300 to 350 ^{o}C at up to 30% steam before degrading. See **Figure 37** for a graphical comparison of experimental versus calculated hydrothermal stability for selected MOFs.

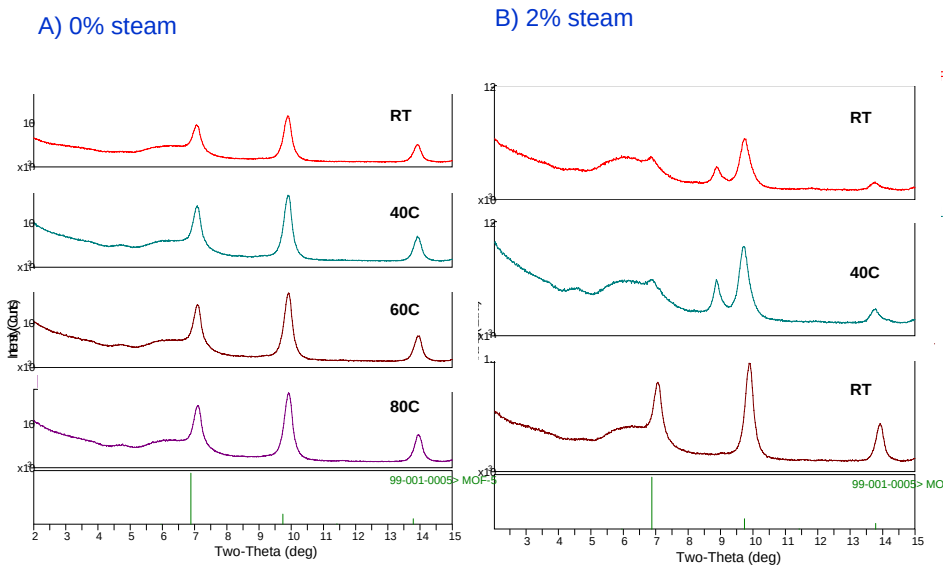

Figure 42. In situ high temperature XRD results for IRMOF-1 in A) no and B) 2% steam environment.

An X-ray diffractometer capable of data collection at elevated temperatures has been equipped with steam-handling capabilities. Outfitted thusly, this instrument enables the *in situ* elucidation of structural feature losses during steaming. Example data are provided as **Figure 42**. Such data reveal the fleeting hydrothermal stability of IRMOF-1. MOF stability toward other contaminants such as SOx and NOx will be examined in detail in the second DOE/NETL sponsored program administered by UOP LLC (DE-FC26-07NT43092).

4.5 Commercial Issues

4.5.1 Background

During the final months of the project, the commercial potential of MOFs in gasifier CO_2 capture was evaluated, and the engineering and economic implications of using the materials in an integrated process were considered. The results of the stability studies performed earlier in the program were critical to help develop flow schemes for the incorporation of MOFs into flue gas and gasification streams. For example, the team conducted a large scale cross validation experiment on IRMOF-1, a benchmark material for carbon dioxide storage and found excellent agreement between experimental sorption isotherms at Michigan and UOP, and with computational studies at Northwestern. These experiments were carried out to support the team Deliverable "Assessment of Commercial Potential" for MOFs in pre-combustion CO_2 capture. A sample of high quality IRMOF-1 was shipped from UM to UOP, and CO_2 adsorption at 311K (~ 100 ^{o}F) was conducted both gravimetrically and volumetrically. Meanwhile, NU generated a simulated CO_2 adsorption isotherm at 311K. The correlation between the two laboratory procedures and one simulation method is excellent (see **Figure 43**).

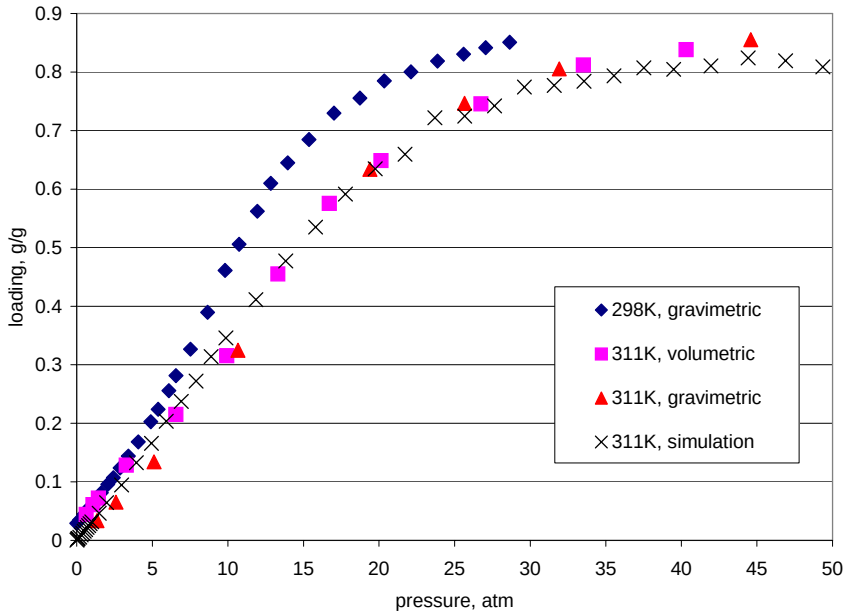

Figure 43. CO_2 adsorption on IRMOF-1 obtained experimentally and simulated. Note exceptional agreement at 311K.

4.5.2 Techno-economic evaluation of the UOP MOF based CO2 capture process

Introduction. While the UOP MOF technology is still in the early stages of development, an attempt has been made to evaluate the capital and operating expenses for a CO_2 capture process from synthesis gas from a gasifier in an IGCC power plant using the MOF material in a pressure swing adsorption (PSA) process. The IGCC technology was chosen for this preliminary techno-economic study because the higher CO_2 partial pressure in the shifted syn gas would be beneficial for an adsorption based process.

Figures 44 and 45 show high level block flow diagrams for the unit operations downstream of the gasifier in IGCC power plants without and with CO_2 capture, respectively.

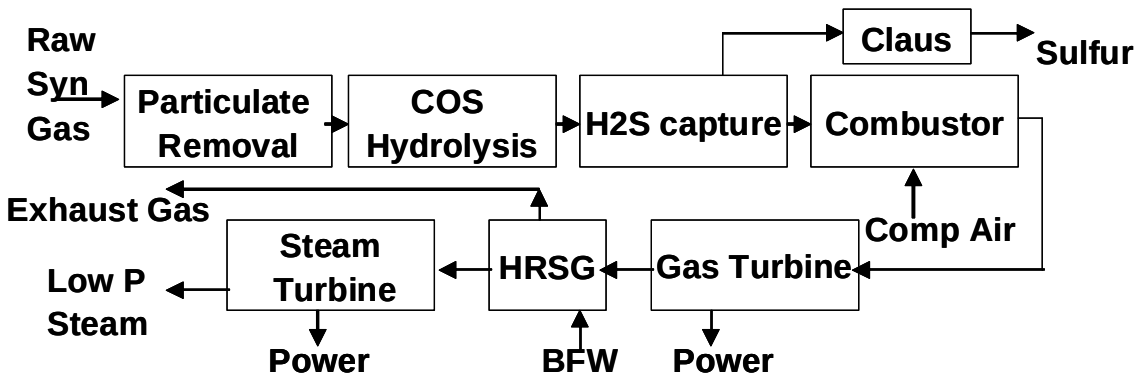

Figure 44. High level block flow diagram without CO_2 capture

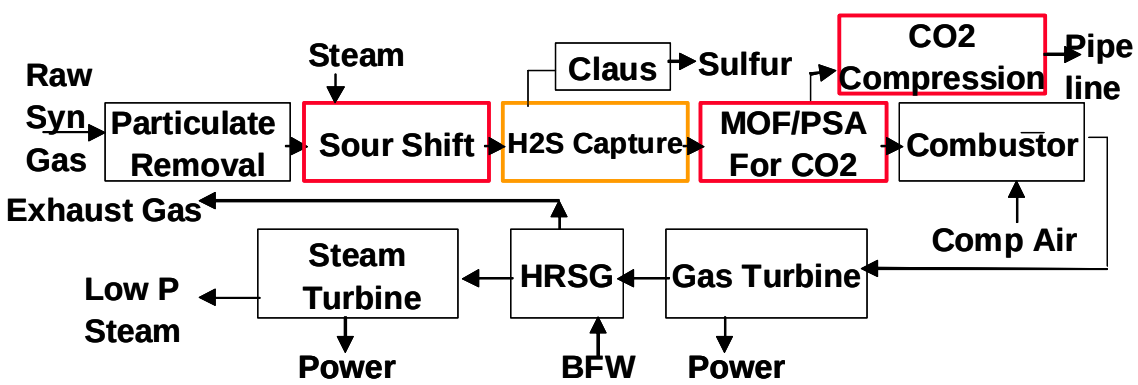

Figure 45. High level block flow diagram with CO_2 capture

For an 85-90% CO_2 (carbon) capture target, one would need three stages of the water gas shift reaction. This study has assumed that this will be a sour shift (i.e., the water gas shift reaction will occur before the removal of H_2S and COS). This eliminates the need for a COS hydrolysis unit that would typically be needed with a solvent based process

such as Selexol because the shift catalyst would also hydrolyze the COS into H2S which is removed more easily by the Selexol solvent. In **Figure 45**, the new plant sections that will be needed to enable CO_2 capture have been marked in red and the section that needs some modifications is marked in orange. The most significant differences between the two flow schemes are as follows:

Capital expenses (CAPEX):

- 3 stages of sour shift to convert CO to CO_2 to achieve target carbon capture
- A slightly bigger H2S capture (Selexol) unit because of the increased flow of CO_2
- A CO_2 capture process which in this case is assumed to be a PSA using the MOF material
- Multi stage compression to raise the pressure of the CO_2 stream to pipeline specifications (152 bara)

Operating expenses (OPEX):

- Lower net power output because of the loss of CO (and CO_2 mass) before the gas turbine
- Steam for the shift reaction
- Power loss for the CO_2 compression

The capital and operating costs for the base IGCC power case without CO_2 capture were taken from the GEE IGCC case in the NETL Fossil Energy Power Plant Desk Reference document[19]. This report assesses the additional capital and operating expenses that would be needed for the conversion, separation and compression of the CO_2 for pipeline.

Basic assumptions. The methodology and assumptions of the NETL Desk Reference were followed unless otherwise noted. These include:

- A plant availability of 80%
- A base case net power output of 640 MW
- A base case Total Plant Cost (TPC) of $1813/KWe
- A base case Busbar cost of 78 mills/KWh
- CO_2 transport, storage and monitoring cost of $4.2/short ton
- A 20 year LCOE capital charge factor of 17.5%
- 20 year LCOE factors for fuel, non-fuel O&M, and fixed O&M of 1.2022, 1.1568, and 1.1568 respectively

The only difference between the NETL Desk Reference (NDR) and this study is that the NDR assumes a carbon capture level of 85%.

The process and project contingency values were applied at the level of the plant sections based on the level of maturity of the technology following the NETL document Carbon Capture and Sequestration Systems Analysis Guidelines from April 2005. A 5% process contingency was applied for all the new sections (mentioned above) except for the MOF/PSA which was given a process contingency value of 20% (since the PSA process

is very well established). The project contingency was assumed to be 14% because of the level of detail assumed in the cost estimates. This is in line with the values of 13.6, 13.7 and 14% used by GEE, CoP and Shell respectively for the IGCC with CO_2 capture cases. In addition, factors from the Carbon Capture and Sequestration Systems Analysis Guidelines were used for calculating the total capital requirement (TCR) and the operating costs.

Methodology and Results. The base case syn gas composition and flow rates were taken from a commercial gasifier case that was available at UOP. Cost estimating approach taken for the different plant sections was as follows:

Sour Shift: Estimated based on private communications with a major vendor of the technology.

COS Hydrolysis: A credit was taken for the capital cost of the COS Hydrolysis unit. This credit was also estimated based on private communications with a major vendor of the technology. No credit was taken for the operating cost of this unit.

Sulfur Removal: Selexol was assumed to be the technology used for H_2S and COS removal (same as in the GEE base case). Two cases were simulated and costed – the base case was for conventional acid gas removal (where the level of CO_2 in the acid gas is not explicitly targeted) and a design case which aimed to retain as much of the CO_2 as possible in the process gas. The cost difference between these two cases was used in this study as the additional cost in the sulfur removal section because of CO_2 capture.

MOF/PSA: A cost estimate was made for a PSA process assuming the CO_2 adsorption properties of MOF-1 at high pressures and 311 K.

Compression: A rule of thumb estimate was used to estimate the capital cost required for CO_2 compression based on the total horse power required for the compression.

The total plant cost (TPC) was estimated to be $183 MM and the total capital requirement (TCR) was estimated to be $225 MM.

Power loss due to CO_2 capture and Sensitivity analysis: A wide range of values have been reported in the literature for the amount of power used/lost during the CO_2 capture process depending on the specific technologies used and the level of energy integration. Given the level of uncertainty in the current study, instead of picking one fixed value for the power used/lost and the TCR, this report studies the impact of these variables on the busbar cost of power.

Transportation, storage and monitoring: A cost of $4.2/short ton of CO_2 sequestered was applied for all the cases. This cost was NOT included in the sensitivity analysis (see above) because it was considered to be beyond the scope of UOP.

Figure 46 shows the impact of the amount of power used/lost due to the CO_2 capture process and the TPC on the busbar cost of power and **Figure 47** shows the impact on the cost per ton of CO_2 removed. **Figures 46 and 47** also show the three IGCC with CO_2 capture cases reported in the NETL Desk Reference.

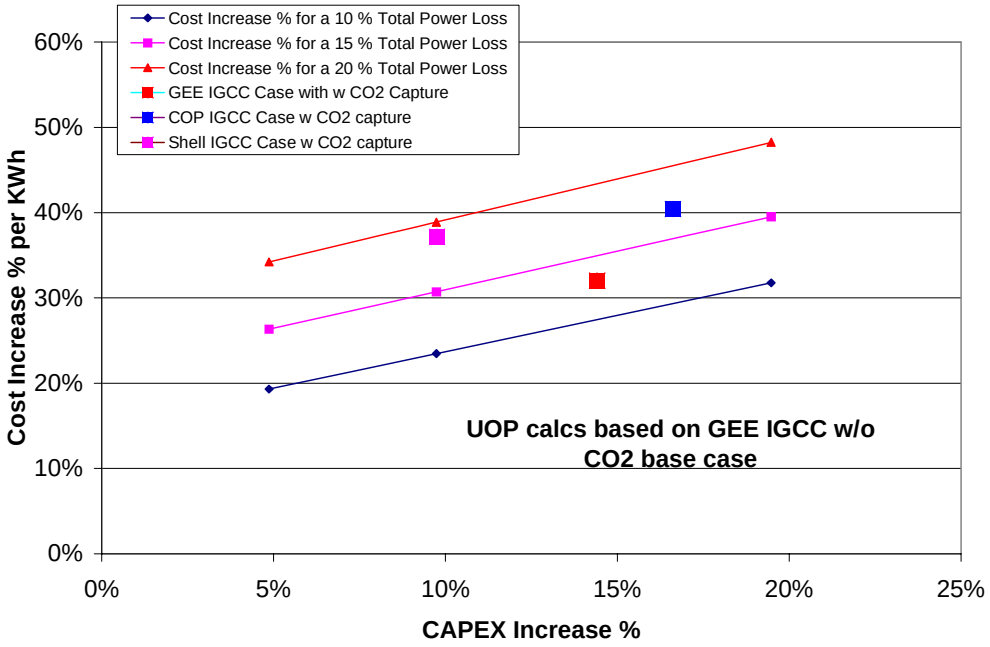

Figure 46. Sensitivity Analysis of Busbar Cost Increase to the CAPEX Increase and Power Loss

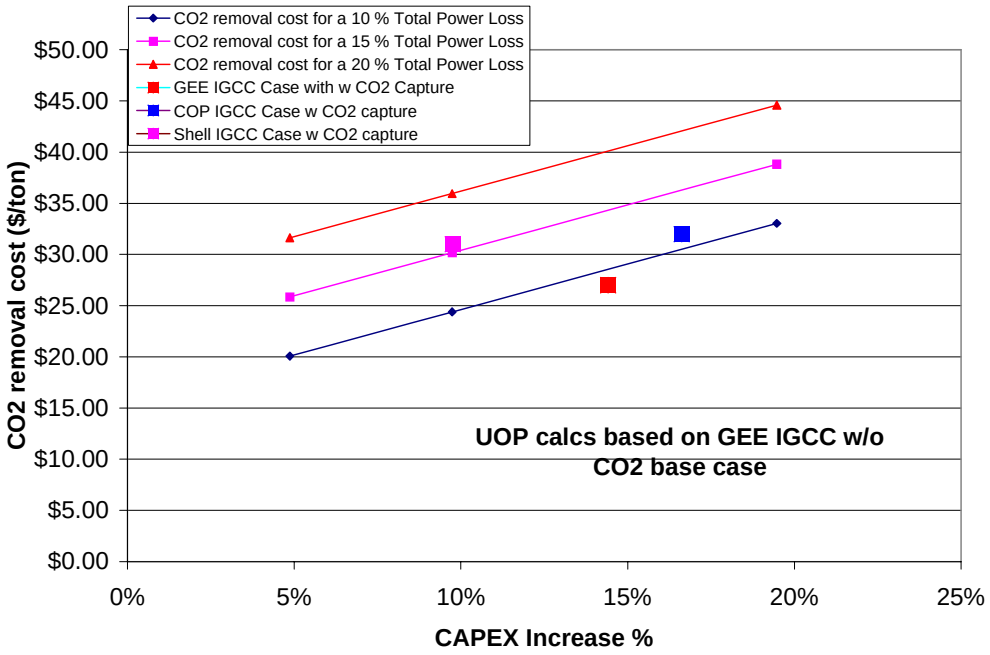

Figure 47. Sensitivity Analysis of CO_2 removal cost to the CAPEX Increase and Power Loss

There are two major results from the analysis. First, the UOP MOF/PSA technology is in the ballpark of the other technologies in the NETL Desk Reference in terms of the cost increase due to CO_2 capture. Part of this is because the energy used in the MOF/PSA section for the capture of CO_2 is lower than the conventional solvent based processes. However, the CO_2 recompression cost could be higher because all the CO_2 rejected from the PSA process is at 3.4 bara while solvent based processes can release at least a fraction of the CO_2 at significantly higher pressures. However, no further conclusions can be drawn given the level of detail in this study.

The second major result is that the amount of power lost due to the CO_2 process has a bigger impact on the busbar cost of power with CO_2 capture than the variability in TCR. If we assume a 100% change in power loss (from 10% to 20%), this leads to an increase in the busbar power cost of 53-79% (depending on the capital cost level), or if we assume a 300% increase in TCR (from 5% to 20%), this leads to an increase in the busbar cost of power of 35-58%, again depending on the power loss level.

Summary. Given these results, one can make the following preliminary conclusions: (1) The cost impact of the MOF/PSA process on the overall CO_2 capture and compression will not be significant because it is only one of many processes that are necessary for capturing CO_2. However, MOFs have an advantage in that they are engineered to be non-toxic (2) There is significant promise on the power used/lost front. Improvements here could include reuse of CO_2 at lower pressure, co-sequestration of CO_2, H_2S and COS, lower purity requirements for CO_2 reuse processes, and better energy integration and optimization of the entire IGCC with CO_2 capture process to best match energy sources and sinks. Such technology exists today but needs to be applied in a more holistic manner.

5 OVERALL CONCLUSIONS

In Phase 1 of the project, reference MOFs were selected based on their structural diversity and projected utility in defining a model for CO_2 capture: IRMOF-1, IRMOF-3, IRMOF-6, MOF-2, MOF-74, and MOF-177. Single component isotherms were completed for CO_2, N_2 and CH_4 for the reference MOFs. An accurate VHTS model was developed to predict isotherms for CO_2 and N_2 on MOFs. Isotherms were calculated for CO_2 and N_2 on IRMOF-1, IRMOF-3, IRMOF-6 and the hydroxyl derivative of IRMOF-1. The end-of-Phase 1 model was used to model separations of CO_2 from other gases.

During Phase 2, several additional conclusions were made. First and foremost, MOFs are promising materials for CO_2 capture. With the exception of MOF-2, the initial reference MOFs show extremely high CO_2 adsorption capacities and very desirable linear isotherm shapes. Second, theory and experiment match very closely. Third, Raman spectroscopy came in handy for the facile characterization of MOF materials. Finally, it was clear that a stronger base functionality will need to be added to MOF linkers in order to enhance CO_2 selectivity over other gases, via, e.g., a chemisorption mechanism.

During early Phase 3, a number of additional conclusions were drawn. First, the preparation of multiple MOF materials from the open literature is a relatively straightforward process. Some of these materials, such as MIL-53, have excellent hydrothermal stability as well as reasonable CO_2 capacity, while others have high CO_2 capacity at modest hydrothermal stability (see **Table 6**). Second, one of our original reference MOFs, MOF-74, has the best CO_2 capacity at atmospheric pressure and ambient temperature. However, MOF-74's hydrothermal stability is fairly good, but not great (**Table 6**). Third, it is clear that linkers outfitted with amine

Table 6. On the road to a MOF for CO_2 capture.

material	**wt% CO2 capacity @ 1 atm**	**wt% CO2 capacity @ 25 atm**	**q (kJ/ mole)**	surface area (sq m/ g)	**pore size (Å)**	relative hydrothermal stability
MOF-74	20	45	35	1100	12	fair
Cu-BTC	19	46	22	2200	4.7 + 10.3 + 12.1	good
MIL-53	10	44	36	1600	5.3	excellent
IRMOF-1	6	100	17	3000	12	bad
MOF-177	3.5	150	NA	4600	20	poor

functionality alone are not sufficiently basic enough to enhance CO_2 adsorption significantly. Fourth, mixed-linker synthesis, utilizing either iso- or non-isomorphous linkers, yields interesting new MOFs. In the non-isomorphous case, a new MOF with built-in mesoporosity (UMCM-1) and another with the highest CO_2 capacity (at 195K) and highest measured surface area for any MOF (UMCM-2), were obtained in high yield.

On the calculational side of the program, we more thoroughly developed the model to predict isotherms for various gases, we calculated the highest possible surface areas for several key MOFs from simulated CO_2 adsorption isotherms, and we developed a new

model to predict MOF stability toward hydrolysis. Predicted stabilities correlated very closely with those observed experimentally via utilization of a high throughput steaming apparatus.

Work during the final months of the project focused on the moisture sensitivity of those MOFs which display the best CO_2 capacity at low pressure and ambient temperatures. UMCM-3 and -4 were discovered, carefully characterized and tested. The Raman spectroscopic method was more fully developed to allow for facile binary adsorption isotherm generation. We also collected data to support the economic and integration assessments, and an assessment of commercial potential for MOFs in IGCC was carried out. General conclusions from the study are that the cost impact of the MOF/PSA process on the overall CO_2 capture and compression will not be significant, and there is significant promise on the power used/lost front. In other words, coupled with other process improvements, MOFs are quite attractive for IGCC CO_2 capture.

The key properties for MOFs to work in this application - *high CO_2 capacity*, *good adsorption/desorption rates*, *high adsorption selectivity* for CO_2 over other gases such as methane and nitrogen, *high stability to contaminants*, namely moisture, and *easy regenerability*, were all addressed to varying degrees during this program.

The three main Deliverables for the project were (a) a MOF for pre-combustion (e.g., IGCC) CO_2 capture, (b) a MOF for post-combustion (flue gas) CO_2 capture, and (c) an assessment of the commercial potential for a MOF in the IGCC application. IRMOF-1, in a bone dry stream, or MIL-53 in a moisture-saturated stream, are two MOFs which could work satisfactorily for the IGCC application. MIL-53 or MOF-74 could work in the flue gas application, but additional work needs to be done to continue the search for an even better low temperature/ low pressure adsorbent. Meanwhile, the preliminary conclusion is that MOFs could be quite suitable for commercial CO_2 capture operations.

6 REFERENCES

[1] (a) J. L. C. Rowsell, O. M. Yaghi, *Angew. Chem. Int. Ed*. **2005**, *44*, 4670; (b) N. W. Ockwig, O. Delgado-Friedriches, M. O'Keefe, O. M. Yaghi, *Acc. Chem. Res*. **2005**, *38*, 176; (c) H. Chae, D. Y. Siberio-Perez, J. Kim, Y. Go, M. Eddaoudi, A. Matzger, M.OKeeffe, O. M. Yaghi, *Nature*, **2004**, *427*, 523; (d) Chae, H. K.; Siberio-Perez, D. Y.; Kim, J.; Go, Y.; Eddaoudi, M.; Matzger, A. J.; O'Keeffe, M.; Yaghi, O. M. *Nature*, **2004**, *427*, 523-527. (e) O. M. Yaghi, M. OKeeffe, N. Ockwig, H. K. Chae, M. Eddaoudi, J. Kim, *Nature*, **2003**, *423*, 705; (f) M. Eddaoudi, J. Kim, N. Rosi, D. Vodak, M. OKeeffe, O. M. Yaghi, *Science*, **2002**, *295*, 469. (g) Li, H.; Eddaoudi, M.; O'Keeffe, M.; Yaghi, O. M. *Nature*, **1999**, *402*, 276-279.

[2] G. Ferey, C. Mellot-Draznieks, C. Serre, F. Millange, *Acc. Chem. Res*. **2005**, *38*, 217; P. M. Forster, A. R. Burbank, C. Livage, G. Ferey, A. K. Cheetham, *Chem. Comm*. **2004**, 368; T. Loiseau, C. Serre, C. Huguenard, G. Fink, F. Taulelle, M. Henry, T. Bataille, G. Ferey, *Chem. Eur. J*. **2004**, *10*, 1373

3 M. Dinca, A. F. Yu, J. R. Long, *J. Am. Chem. Soc*. **2006**, *128*, 8904; X. Guo, G. Zhu, Z. Li, F. Sun, Z. Yang, S. Qui, *Chem. Comm*. **2006**, 3172; R. Matsua, R. Kitaura, S. Kitagawa, Y. Kubota, R. V. Belosludov, T. C. Kobayashi, H. Sakamoto, T. Chiba, M. Takata, Y. Kawazoe, Y. Mita, *Nature* **2005**, *436*, 238; D. N. Dybtsev, H. Chun, S. H. Yoon, D. Kim, K. Kim, *J. Am. Chem. Soc*. **2004**, *126*, 32.

[4] Koh, K., Wong-Foy, A.G., Matzger, A.J., *Angew. Chem*. **2008**, *47*, 677.

[5] Rowsell, J.L.C.; Yaghi, O.M., *J. Am. Chem. Soc*. **2006**, *128*, 1304, and references therein.

[6] Sing, K. S. W.; Everett, D. H.; Haul, R. A. W.; Moscou, L.; Pierotti, R. A.; Rouquerol, J.; Siemieniewska, T. *Pure & Appl. Chem.* **1985**, *57*, 603-619.

[7] J.J. Potoff, J.I. Siepmann, *AIChE J.* **2001**, 47, 1676.

[8] S.L. Mayo, B.D. Olafson, W.A. Goddard III, *J. Phys. Chem.* **1990**, 94, 8897.

[9] T. Düren, L. Sarkisov, O.M. Yaghi, R.Q. Snurr, *Langmuir* **2004**, *20*, 2683.

[10] H. Frost, T. Düren, R.Q. Snurr, *J. Phys. Chem. B* **2006**, *110*, 9565.

[11] K.S. Walton, A.R. Millward, D. Dubbeldam, H. Frost, J.J. Low, O.M. Yaghi, R.Q. Snurr, *J. Am. Chem. Soc.* **2008**, *130*, 406.

[12] S.S.Y. Chui, S.M.F. Lo, J.P.H. Charmant, A.G.Orpen, I.D. Williams, *Science* **1999**, *283*, 1148.

[13] B. Chen, M. Eddaoudi, T.M. Raineke, J.W. Kampf, M. O'Keeffe, O.M. Yaghi, *J. Am. Chem. Soc.* **2000**, *118*, 11559.

[14] X. Guo, G.Zhu, Z. Li, F.Sun, Z.Yang, S.Qiu, *Chem. Comm.* **2006**, *30*, 3172.

[15] J.A.R. Navarro, E.Barea, J.M. Salas, N. Masciocchi, S. Galli, A. Sironi, C.O Ania, J.B. Parra, *Inorg. Chem* **2006**, *45*, 2397.

[16] Walton, K.S., Snurr, R.Q. *J. Am. Chem. Soc.* **2007**, *129*, 8552

[17] J. A. Greathouse, and M. D. Allendorf, *J. Am. Chem. Soc.* **2006**, *128*, 10678.

[18] (a) B. Delley, *J. Chem. Phys.* **1990**, *92*, 508; (b) B. Delley, *J. Chem. Phys.* **2000**, *113*, 7756. $DMol^3$ is available as part of Materials Studio from Accelrys Inc. Version 4.2.1. The DN basis set and medium precision was used in these calculations.

[19] DOE/NETL-2007/1282, May **2007**